



Vibration stabilization by a nonresonant secondary limit cycle oscillator

D. D. Tandel · Pankaj Wahi ·
Anindya Chatterjee

Received: 30 March 2022 / Accepted: 26 November 2022 / Published online: 11 December 2022
© The Author(s), under exclusive licence to Springer Nature B.V. 2022

Abstract Many vibrating systems, over some ranges of parameter values, exhibit a single unstable mode. Adding a small resonant secondary system to the unstable system is a well-known stabilization strategy. Here we show that even a nonresonant secondary system, if equipped with a limit cycle of its own, can stabilize the unstable mode of the primary system. The primary system is modeled here as a linear spring block system with negative damping. The secondary system is a van der Pol oscillator. Smallness of the latter's parameters allows use of the method of multiple scales. The resulting slow amplitude equations decouple from the phases and a two-dimensional system is obtained. The secondary system's amplitude evolves faster than that of the primary system, which simplifies analysis. A parameter-dependent transformation casts the system in a canonical form with a single free parameter $c_1 > 0$ in addition to the small perturbation parameter. The canonical phase portrait involves two key straight lines. When $c_1 < 4$ these lines intersect and a separatrix passes through that intersection. Solutions on one side of the separatrix show quenching of the primary

instability with limit cycle oscillation of the secondary system. Solutions on the other side of the separatrix show significant oscillations of the primary system at its natural frequency, with the secondary limit cycle being quenched. When $c_1 > 4$, stabilization fails for all initial conditions. In summary, for the case of a negatively damped oscillator interacting with a small nonresonant secondary limit cycle oscillator, we show stabilization, provide a pair of canonical equations with one free parameter, and present a complete qualitative characterization of the dynamics.

Keywords Negative damping · Stabilization · van der Pol oscillator · Multiple scales · Separatrix

1 Introduction

Stabilization of unstable vibration modes is an important engineering problem. Structures exposed to aerodynamic loading can experience flutter instability. High tension transmission lines exposed to winds can show what is called a galloping instability. Long, flexible members of machine tools, like boring bars, can display undesirable oscillations while cutting. Here we consider a single mode of such a weakly unstable structure as our primary system and model it as a linear spring-mass oscillator with, for simplicity, negative linear viscous damping. There is no persistent external excitation. Our aim is to counteract the negative damping and stabilize the mode.

D. D. Tandel (✉) · P. Wahi · A. Chatterjee
Mechanical Engineering, Indian Institute of Technology,
Kanpur, U.P. 208016, India
e-mail: ddtandel@iitk.ac.in

Pankaj Wahi
e-mail: wahi@iitk.ac.in

Anindya Chatterjee
e-mail: anindya@iitk.ac.in
e-mail: anindya100@gmail.com

Our main novelty in this paper is that we do not use resonance, because that requires precise tuning. We are interested in a stabilizer that does not require precise tuning.

To that end, we consider attaching a small secondary system to the primary system, wherein the secondary system's natural frequency is *not close* to that of the primary system, i.e., the secondary system is untuned. Additionally, the secondary system has its own nonlinear active behavior that we model using the well-known van der Pol oscillator. In this way, the small and light secondary system has a tendency to vibrate at one frequency, while the more massive primary system has a tendency to vibrate at another frequency altogether. The aim of our investigation is to seek new analytical criteria, with proper numerical support, for conditions under which the instability in the primary system is suppressed. If we succeed, then we will have found a new kind of vibration stabilizer which is robust under parameter uncertainty, because precise tuning of the frequency is not needed. The price paid will be the active excitation of the secondary system: but this will not require feedback of the primary system state.

When we try to stabilize vibrations, we can do it with passive damping which is not tuned at all, and is effective over a large range of frequencies. However, it has the disadvantage that, for a large structure, a physically large damper may be needed. Another option is active control where we measure the state of the system and feed back something to an actuator, where again, a physically large actuator may be needed. In contrast, if we use passive dynamic methods, we may have a tuned vibration absorber, and it can be extremely effective in some cases. However, the parameters of the stabilized system must then remain within a narrow range. For example, if a boring bar is gripped at different locations, its effective length and natural frequency may change too much, and a tuned vibration absorber will then be less effective. In contrast to the above approaches, in this paper, we seek something that does not require *precise* tuning, is physically small, and still is effective over a larger range of natural frequencies of the primary oscillator, i.e., it does not require a resonant interaction to work. We emphasize that the resonant case, when it works, works very well. However, when resonance cannot be maintained due to parameter variations, a nonresonant stabilizer can be considered. We note that in the present paper, although we envisage the use of active means to produce a limit cycle oscilla-

tion in the secondary system, it is less demanding than using direct feedback on the primary system because the secondary system size and actuator size are both expected to be small. Detailed modeling of the physical mechanisms used to produce the secondary limit cycle is left to future work. In this paper we work out the basic academic theory.

In our two-degree-of-freedom system, both modes have negative damping in the linearized equations. So there will essentially be a contest between two instabilities. Since the secondary system is small, its effect will only be felt if the initial conditions for the primary system are small as well. However, as we will show, significant regimes of desirable behavior may be possible for initial conditions of usefully large size.

2 Literature review

The broad context in which we present our work is as follows. Traditional tuned mass dampers (TMDs) are well-known passive absorbers in the vibrations research community. Improvements in TMD have continued long after its introduction by Frahm in 1911 [1]. The advantage of passive vibration absorbers is that they do not require any external power source. However, TMDs have the disadvantage of being effective only in a narrow frequency range. Researchers continue to design and improve vibration absorbers effective over a wider range of frequencies. Ibrahim [2] has documented the history of passive vibration absorbers. With an introduction of nonlinearity in TMDs, nonlinear vibration absorbers (NVAs) or nonlinear energy sinks (NESs) have gained attention as potential candidates to replace TMDs. While they involve challenges like multivaluedness (or multiple steady state behaviors) and instability in some cases, NESs can offer the advantage of having a broader working frequency range than TMDs. Ding and Chen [3] have reviewed NES designs and applications.

Since our primary structure is a linear spring-mass oscillator while our secondary oscillator is nonlinear, we specifically mention some articles in which an NES is attached to a linear oscillator. Gatti [4] considered an NES with a linear and cubic spring nonlinearity and viscous damping attached to a damped linear spring-mass system subjected to harmonic forcing. Using frequency response analysis, tuning conditions were presented to apply the NES as an absorber or a neutralizer depend-

ing on the forcing frequency, considering the hardening and softening characteristics of the cubic spring. Although the attenuation observed for the desired forcing frequency remained similar to that using a linear attachment, bandwidth improvement was recognized. Starosvetsky and Gendelman [5] investigated an NES with nonlinear damping and a pure cubic spring element attached to a linear spring-mass system under periodic forcing. They showed that the introduction of damping nonlinearity could annihilate undesirable nonlinear effects, i.e., extending the amplitude of forcing over which the NES is effective. Zhu et al. [6] studied a two-degree-of-freedom system with nonlinear spring and damper elements in primary and secondary systems, where the latter is excited. Using frequency response curves, they showed that increasing the secondary oscillator's nonlinear spring and damping coefficients improves attenuation while increasing the primary system's nonlinear parameters serves when a nondimensional forcing frequency (defined therein) is below unity. It is important to note that these studies related to the enhancement of TMDs and NESs have focused on vibration mitigation of periodically forced structures. Attempts towards suppression of self-excited oscillations can be found in [7, 8] and [9]. Verhulst [7] studied quenching of self-excited oscillations in the van der Pol and Rayleigh oscillators by coupling another oscillator. As a tuning methodology, coupling parameters were chosen such that the stable periodic solution of the self-excited oscillator became unstable. For strong interaction, quenching of relaxation oscillations was attempted, and design recommendations were given. Lee et al. [8] investigated the efficacy of an NES with essentially nonlinear cubic spring and viscous damping in suppressing limit cycle oscillations of the van der Pol oscillator for grounded and ungrounded configurations. They showed that elimination of the limit cycle of the primary structure is attainable. Habib and Kerschen [9] studied mitigation of limit cycles in the van der Pol-Duffing oscillator. The attached nonlinear tuned vibration absorber (NLTVA) has linear and cubic spring elements with viscous damping. The optimum value of the frequency ratio of the linear parts of both oscillators was close to unity, i.e., tuning was needed. Additional benefits from nonlinearity were noted.

We now focus our literature review to some papers that specifically included linear viscous negative damping in the primary oscillator. Such papers include many

that refer to flow-induced vibrations. Passive vibration absorbers for flow-induced vibrations have been studied for decades: see the review paper by Wang et al. [10]. Nasrabadi et al. [11] studied design of an NES for vibration suppression of a cantilever cylinder under cross-flow. They achieved significant reduction in the vibration amplitude of the cylinder. Guo et al. [12] studied the suppression of limit cycle oscillation of a linear extensible cable. They showed that an NES can raise the wind speed needed for initiation of galloping. The role of attachment location was studied as well. Qin et al. [13] studied models of a transmission line with one through three degrees of freedom. The secondary system was a pendulum, and the roles of length, mass, and damping were studied. Tuning was found to be beneficial. Dai et al. [14] studied the use of an NES to suppress fluid-induced vibrations of a single degree of freedom (SDOF) system. It was found that damping plays a strong role, and a stronger nonlinear stiffness can limit response amplitudes more effectively. Shirude et al. [15] also studied an essentially nonlinear vibration stabilizer for a negatively damped SDOF system. They used informal harmonic balance-based averaging to obtain both steady state responses and stability information. The stabilizer was found to be effective for some range of parameter values, and precise tuning was not needed. In all the papers referred to in this paragraph, the response of the secondary system, whether it is weakly or strongly nonlinear, and tuned or untuned, was essentially at the natural frequency of the primary system.

In a rather different approach from those above, Singla and Chatterjee [16] studied a negatively damped linear system coupled with a light whirling viscously damped pendulum driven by a small steady torque. In the stabilized regime, the pendulum frequency was *not tuned* to the primary oscillator. The method of multiple scales, carried out to second-order, gave an analytical stability criterion which was then supported by numerics. Post-instability behavior was also studied, but is not relevant to the present work. The whirling pendulum system differs from other NESs in that it has constant amplitude and specific untuned frequency. That paper [16] motivates our present work, where we incorporate the preferred amplitude approximately and are able to eliminate the need for a whirling pendulum component.

Finally, we acknowledge papers [17–19] which, although not identical to our work, share some philosophical similarities. Chatterjee [17] considered lin-

ear control actuation of a secondary oscillator coupled to a self-excited primary system with nonlinear damping. Given absorber parameters including the absorber's natural frequency, optimum feedback gains were found. It was noted that higher absorber frequencies gave greater robustness. Since the primary system is nonlinearly self-excited and the feedback parameters are both linear and based on inertial position and velocity of the absorber mass, the system deviates from ours. Additionally, the total dynamics in [17] could not be reduced to a simple one-parameter form as we will present here. Mondal and Chatterjee [18] applied resonant nonlinear feedback control to suppress self-excited oscillations in a single-mode nonlinear model of a beam. The velocity measurement from the beam was fed to a second-order filter (which is essentially a damped harmonic oscillator), and then the filtered velocity (which is essentially the velocity of that secondary oscillator) was used to provide feedback control. Here also, the primary system was self-excited and nonlinear; and eventually the optimum frequency of the secondary system was found to be equal to the natural frequency of the original system, i.e., the optimum system was resonant. Third, we come to the work of Gattulli et al. [19]. This work has somewhat greater relevance to our work, as will become clearer below. The work of [19] is discussed in greater detail in Sects. 3 and 6. Finally, at the suggestion of an anonymous reviewer, we acknowledge that many studies are available related to the van der Pol oscillator coupled to either the van der Pol, the Duffing or some other oscillator. For this reason, we have conducted a broader literature review and categorized many such articles based on their focus of study. That discussion is given in Appendix A. We conclude our literature review here by highlighting the main characteristics of the stabilizer proposed in the present study as being *light*, *nonresonant* and *self-excited*.

3 Equations of motion

Figure 1 shows a schematic of the system considered in this paper. We consider a primary oscillator with mass M , spring stiffness K and viscous damping coefficient C . A negative value of C represents instability in the primary structure. The attached van der Pol (sometimes called “vdP”) oscillator has mass \bar{m} , linear spring stiffness \bar{k} and nonlinear damping coefficient \bar{c}_v , while x

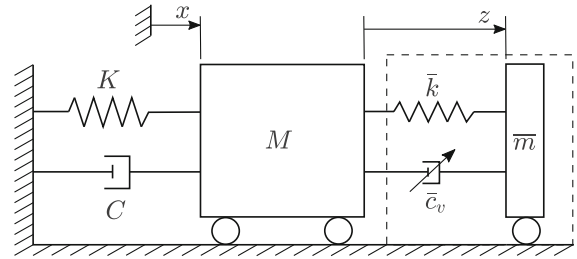


Fig. 1 Schematic of the coupled system

and z denote the absolute and relative displacements of the primary and secondary systems, respectively. The equations of motion (EOMs) are

$$M\ddot{x} + C\dot{x} + Kx - \bar{k}z - \bar{c}_v\dot{z}(z^2 - 1) = 0, \quad (1)$$

$$\bar{m}(\ddot{z} + \ddot{x}) + \bar{k}z + \bar{c}_v\dot{z}(z^2 - 1) = 0, \quad (2)$$

By either choice of units or a preliminary nondimensionalization, we can set $M = 1$ and $K = 1$ to obtain

$$\ddot{x} + \tilde{C}\dot{x} + x - \tilde{k}z - \tilde{c}_v\dot{z}(z^2 - 1) = 0,$$

$$\tilde{m}(\ddot{z} + \ddot{x}) + \tilde{k}z + \tilde{c}_v\dot{z}(z^2 - 1) = 0,$$

where \tilde{C} , \tilde{m} , \tilde{c}_v and \tilde{k} are nondimensional parameters given by

$$\tilde{C} = \frac{C}{\sqrt{MK}}, \quad \tilde{m} = \frac{\bar{m}}{M}, \quad \tilde{c}_v = \frac{\bar{c}_v}{\sqrt{MK}}, \quad \tilde{k} = \frac{\bar{k}}{K}. \quad (3)$$

Note that the nondimensional time sets the natural frequency of the primary oscillator to unity. Now, we introduce a small bookkeeping parameter ε and write

$$\tilde{C} = \varepsilon c, \quad \tilde{m} = \sqrt{\varepsilon} m, \quad \tilde{c}_v = \varepsilon c_v \quad \text{and} \quad \tilde{k} = \sqrt{\varepsilon} k, \quad (4)$$

The parameters c , m , c_v and k are understood to be $\mathcal{O}(1)$. We will not refer to the unscaled quantities any more. The EOMs take the form

$$\ddot{x} + \varepsilon c\dot{x} + x - \sqrt{\varepsilon} k z - \varepsilon c_v \dot{z}(z^2 - 1) = 0,$$

$$\sqrt{\varepsilon} m(\ddot{z} + \ddot{x}) + \sqrt{\varepsilon} k z + \varepsilon c_v \dot{z}(z^2 - 1) = 0.$$

We define

$$\omega_p^2 = \frac{k}{m} \quad \text{and} \quad \gamma = \frac{c_v}{m} \quad (5)$$

for convenience, obtaining

$$\ddot{x} + \varepsilon c \dot{x} + x - \sqrt{\varepsilon} m \omega_p^2 z - \varepsilon m \gamma \dot{z}(z^2 - 1) = 0, \tag{6}$$

$$\ddot{z} + \ddot{x} + \omega_p^2 z + \sqrt{\varepsilon} \gamma \dot{z}(z^2 - 1) = 0. \tag{7}$$

We will study Eqs. (6) and (7) using the method of multiple scales in the next section.

We are now in a position to discuss the work of Gattulli et al. [19], who studied the effect of a tuned mass damper (TMD) on a single degree of freedom model of a bluff body undergoing galloping. Their nondimensionalized equations (Eq. (4) in [19]) are

$$\ddot{q}_1 + 2\xi \dot{q}_1 + 2\mu\gamma\xi_t(\dot{q}_1 - \dot{q}_2) + q_1 + \mu\gamma^2(q_1 - q_2) = \delta \frac{A_3}{U} \dot{q}_1^3,$$

$$\ddot{q}_2 + 2\gamma\xi_t(\dot{q}_2 - \dot{q}_1) + \gamma^2(q_2 - q_1) = 0.$$

Writing $z = q_2 - q_1$, we obtain

$$\ddot{q}_1 + 2\xi \dot{q}_1 - 2\mu\gamma\xi_t \dot{z} + q_1 - \mu\gamma^2 z = \delta \frac{A_3}{U} \dot{q}_1^3,$$

$$\ddot{q}_1 + \ddot{z} + 2\gamma\xi_t \dot{z} + \gamma^2 z = 0.$$

We note that the parameter values mentioned in [19] are $2\xi = -0.1356$ and $\delta \frac{A_3}{U} = -0.0033$ with $\delta = 4.7 \times 10^{-4}$, $A_3 = -421$, $U \sim 60$. Because the RHS in the first equation is small for the reported parameter values, and it only modifies the damping, we drop it to obtain

$$\ddot{q}_1 + 2\xi \dot{q}_1 - 2\mu\gamma\xi_t \dot{z} + q_1 - \mu\gamma^2 z = 0,$$

$$\ddot{q}_1 + \ddot{z} + 2\gamma\xi_t \dot{z} + \gamma^2 z = 0.$$

Now, to connect with our system, we introduce a van der Pol term instead of the linear damping term, to obtain

$$\ddot{q}_1 + 2\xi \dot{q}_1 - 2\mu\gamma\xi_t(z^2 - 1)\dot{z} + q_1 - \mu\gamma^2 z = 0,$$

$$\ddot{q}_1 + \ddot{z} + 2\gamma\xi_t(z^2 - 1)\dot{z} + \gamma^2 z = 0.$$

The above equations match our Eqs. (6) and (7) if we rename the parameters appropriately. In this way, it is clear that if the van der Pol term is achieved using relatively small components and active control, then the results of our paper are relevant to practical systems studied by other researchers in the nonlinear dynamics community. In fact, the authors of [19] continued with a study of the above system after including a $z^2\dot{z}$ term in [20], which makes the connection with the van der Pol oscillator more direct. However, in [20], the two oscillators were resonant, while in our system they are not resonant.

We now return to an analysis of our equations.

4 Multiple scales analysis

The method of multiple scales is an asymptotic method which transforms an ordinary differential equation into a partial differential equation by considering different time scales to be independent variables within an assumed functional form [21,22]. The method has been regularly applied to a wide variety of engineering and physics problems. The reader may also refer to the review paper by Cartmell et al. [23] to appreciate features of the method in the context of weakly nonlinear mechanical systems. Here we apply multiple scales analysis up to second-order to obtain good approximations for the system dynamics. The intermediate expressions are lengthy but can be handled by the computer algebra package Maple, and the final evolution equations are simple and easy to interpret.

The reader may note that, although the multiple scales method presents a seemingly unified approach to a large variety of problems, there may be important differences in the detailed applications to different classes of problems. In terms of the analytical treatment of resonant versus nonresonant interactions, such is indeed the case. When we have a resonant system, we use a detuning parameter. And usually, first-order multiple scales or first-order averaging will give us a useful slow flow. However, when we do nonresonant analysis, usually we have to go to second order to obtain a nontrivial term, and the slow flows obtained are not at all easy to predict from intuition. The expressions dealt with are much longer as well, but it is possible to handle them using symbolic algebra packages. For these reasons, in principle, in detail, and in the magnitude of calculations involved, the resonant and the nonresonant analyses are quite different.

4.1 Initial setup

We let $\mu = \sqrt{\varepsilon}$ and rewrite Eqs. (6) and (7) as

$$\begin{aligned} \ddot{x} + \mu^2 c \dot{x} + x - \mu m \omega_p^2 z - \mu^2 m \gamma \dot{z}(z^2 - 1) &= 0, \\ \ddot{z} + \ddot{x} + \omega_p^2 z + \mu \gamma \dot{z}(z^2 - 1) &= 0. \end{aligned}$$

We introduce multiple time scales $T_0 = t$, $T_1 = \mu t$ and $T_2 = \mu^2 t$; and then expand $x = X_0 + \mu X_1 + \mu^2 X_2$ and $z = Z_0 + \mu Z_1 + \mu^2 Z_2$. Substituting these expansions into the above equations, we obtain at $\mathcal{O}(1)$

$$\frac{\partial^2}{\partial T_0^2} X_0(T_0, T_1, T_2) + X_0(T_0, T_1, T_2) = 0, \tag{8}$$

$$\begin{aligned} &\frac{\partial^2}{\partial T_0^2} Z_0(T_0, T_1, T_2) + \omega_p^2 Z_0(T_0, T_1, T_2) \\ &+ \frac{\partial^2}{\partial T_0^2} X_0(T_0, T_1, T_2) = 0. \end{aligned} \tag{9}$$

Solving Eq. (8) for X_0 , we obtain

$$X_0(T_0, T_1, T_2) = R(T_1, T_2) \sin(T_0 + \phi(T_1, T_2)). \tag{10}$$

In the above, R denotes the $\mathcal{O}(1)$ amplitude of the primary oscillator. We substitute the above $X_0(T_0, T_1, T_2)$ into Eq. (9) and obtain

$$\begin{aligned} &\frac{\partial^2}{\partial T_0^2} Z_0(T_0, T_1, T_2) + \omega_p^2 Z_0(T_0, T_1, T_2) \\ &- R(T_1, T_2) \sin(T_0 + \phi(T_1, T_2)) = 0. \end{aligned} \tag{11}$$

We solve Eq. (11) for Z_0 and obtain

$$\begin{aligned} Z_0(T_0, T_1, T_2) = &Q(T_1, T_2) \sin(\omega_p T_0 + \psi(T_1, T_2)) \\ &- \frac{R(T_1, T_2) \sin(T_0 + \phi(T_1, T_2))}{(1 - \omega_p^2)}, \end{aligned} \tag{12}$$

where the first term with new slowly-evolving variables $Q(T_1, T_2)$ and $\psi(T_1, T_2)$ is a complementary solution, and the second term is the particular integral. From the latter, $\omega_p \neq 1$, i.e., $m \neq k$ (by Eq. (5)) in the van der Pol oscillator, is an obvious requirement for the analysis to proceed. We recall that $(x + z)$ is the absolute displacement of the secondary oscillator. By Eqs. (10) and (12), Q denotes the $\mathcal{O}(1)$ amplitude of $z + \frac{x}{1 - \omega_p^2}$.

When the primary system is stabilized, i.e., x is small or even zero, Q represents the amplitude of the secondary oscillator. In what follows, we suppress the (T_0, T_1, T_2) dependence of already-introduced quantities for compact representation.

4.2 Intermediate details

Although the method of multiple scales is well known, here the presence of two frequencies makes some things somewhat new. For completeness, details are presented in this subsection and analysis of the slow dynamics proceeds in the next subsection.

Proceeding as usual, we obtain at $\mathcal{O}(\mu)$

$$\begin{aligned} &\frac{\partial^2 X_1}{\partial T_0^2} + X_1 + \left(2 \frac{\partial R}{\partial T_1}\right) \cos(T_0 + \phi) \\ &+ \left(-2 \frac{\partial \phi}{\partial T_1} + \frac{m \omega_p^2}{1 - \omega_p^2}\right) R \sin(T_0 + \phi) \\ &- m \omega_p^2 Q \sin(\omega_p T_0 + \psi) = 0, \end{aligned} \tag{13}$$

and

$$\begin{aligned} &\frac{\partial^2 Z_1}{\partial T_0^2} + \omega_p^2 Z_1 + \frac{\partial^2 X_1}{\partial T_0^2} + \frac{\omega_p}{4(1 - \omega_p^2)^2} \\ &\left(\gamma(1 - \omega_p^2)^2 Q^3 + 2\gamma(R^2 - 2(1 - \omega_p^2)^2) Q \right. \\ &\left. + 8(1 - \omega_p^2)^2 \frac{\partial Q}{\partial T_1}\right) \cos(\omega_p T_0 + \psi) \\ &- 2Q \omega_p \frac{\partial \psi}{\partial T_1} \sin(\omega_p T_0 + \psi) - \frac{1}{4(1 - \omega_p^2)^3} \\ &\left(2\gamma(1 - \omega_p^2)^2 Q^2 R + \gamma(R^2 - 4(1 - \omega_p^2)^2) R \right. \\ &\left. + 8(1 - \omega_p^2)^2 \omega_p^2 \frac{\partial R}{\partial T_1}\right) \cos(T_0 + \phi) \\ &+ \frac{2R \omega_p^2}{(1 - \omega_p^2)} \frac{\partial \phi}{\partial T_1} \sin(T_0 + \phi) \\ &+ \frac{\gamma(2 - \omega_p) Q R^2}{4(1 - \omega_p^2)^2} \cos(2T_0 - \omega_p T_0 + 2\phi - \psi) \\ &+ \frac{\gamma R^3}{4(1 - \omega_p^2)^3} \cos(3T_0 + 3\phi) \\ &+ \frac{\gamma(1 + 2\omega_p) Q^2 R}{4(1 - \omega_p^2)} \cos(T_0 + 2\omega_p T_0 + \phi + 2\psi) \\ &- \frac{1}{4} \gamma \omega_p Q^3 \cos(3\omega_p T_0 + 3\psi) \\ &- \frac{\gamma(2 + \omega_p) Q R^2}{4(1 - \omega_p^2)^2} \cos(2T_0 + \omega_p T_0 + 2\phi + \psi) \\ &+ \frac{\gamma(1 - 2\omega_p) Q^2 R}{4(1 - \omega_p^2)} \cos(T_0 - 2\omega_p T_0 + \phi - 2\psi) \\ &= 0. \end{aligned} \tag{14}$$

To eliminate secular terms in Eq. (13), assuming ω_p is not close to $1/3$ for reasons that will be clear below, we require

$$2 \frac{\partial R}{\partial T_1} = 0, \tag{15}$$

and

$$\left(-2 \frac{\partial \phi}{\partial T_1} + \frac{m \omega_p^2}{1 - \omega_p^2}\right) R = 0. \tag{16}$$

Because $R \neq 0$ in general, by Eqs. (15) and (16), we conclude

$$R(T_1, T_2) = R(T_2), \tag{17}$$

and

$$\frac{\partial \phi}{\partial T_1} = \frac{m \omega_p^2}{2(1 - \omega_p^2)}. \tag{18}$$

We incorporate the conclusions (17) and (18) into Eq. (13), and obtain

$$\frac{\partial^2 X_1}{\partial T_0^2} + X_1 - m\omega_p^2 Q \sin(\omega_p T_0 + \psi) = 0. \tag{19}$$

Solving Eq. (19) for X_1 , we obtain

$$X_1(T_0, T_1, T_2) = \frac{m\omega_p^2}{1 - \omega_p^2} Q \sin(\omega_p T_0 + \psi), \tag{20}$$

where we have dropped the complementary solution because we are not solving an initial value problem and Eq. (10) contains the complementary solution already. We substitute the solution for X_1 , i.e., Eq. (20), into Eq. (14) and obtain

$$\begin{aligned} & \frac{\partial^2 Z_1}{\partial T_0^2} + \omega_p^2 Z_1 + \frac{\omega_p}{4(1 - \omega_p^2)^2} \\ & \left(\gamma(1 - \omega_p^2)^2 Q^3 + 2\gamma(R^2 - 2(1 - \omega_p^2)^2) Q \right. \\ & \left. + 8(1 - \omega_p^2)^2 \frac{\partial Q}{\partial T_1} \right) \cos(\omega_p T_0 + \psi) \\ & - \left(2 \frac{\partial \psi}{\partial T_1} + \frac{m\omega_p^3}{(1 - \omega_p^2)} \right) \omega_p Q \sin(\omega_p T_0 + \psi) \\ & - \frac{1}{4(1 - \omega_p^2)^3} \left(2\gamma(1 - \omega_p^2)^2 Q^2 R \right. \\ & \left. + \gamma(R^2 - 4(1 - \omega_p^2)^2) R + 8(1 - \omega_p^2)^2 \omega_p^2 \frac{\partial R}{\partial T_1} \right) \\ & \cos(T_0 + \phi) + \frac{2R\omega_p^2}{(1 - \omega_p^2)} \frac{\partial \phi}{\partial T_1} \sin(T_0 + \phi) \\ & + \frac{\gamma R^3}{4(1 - \omega_p^2)^3} \cos(3T_0 + 3\phi) \\ & + \frac{\gamma(1 + 2\omega_p) Q^2 R}{4(1 - \omega_p^2)} \cos(T_0 + 2\omega_p T_0 + \phi + 2\psi) \\ & - \frac{1}{4} \gamma \omega_p Q^3 \cos(3\omega_p T_0 + 3\psi) \\ & + \frac{\gamma(1 - 2\omega_p) Q^2 R}{4(1 - \omega_p^2)} \cos(T_0 - 2\omega_p T_0 + \phi - 2\psi) \\ & - \frac{\gamma(2 + \omega_p) Q R^2}{4(1 - \omega_p^2)^2} \cos(2T_0 + \omega_p T_0 + 2\phi + \psi) \\ & + \frac{\gamma(2 - \omega_p) Q R^2}{4(1 - \omega_p^2)^2} \cos(2T_0 - \omega_p T_0 + 2\phi - \psi) \\ & = 0. \end{aligned} \tag{21}$$

To eliminate secular terms in Eq. (21), we require

$$\frac{\omega_p}{4(1 - \omega_p^2)^2} \left(\gamma(1 - \omega_p^2)^2 Q^3 \right.$$

$$\left. + 2\gamma(R^2 - 2(1 - \omega_p^2)^2) Q + 8(1 - \omega_p^2)^2 \frac{\partial Q}{\partial T_1} \right) = 0, \tag{22}$$

and

$$\left(2 \frac{\partial \psi}{\partial T_1} + \frac{m\omega_p^3}{(1 - \omega_p^2)} \right) \omega_p Q = 0. \tag{23}$$

Because $Q \neq 0$ in general, by Eqs. (22) and (23), we find

$$\frac{\partial Q}{\partial T_1} = - \frac{\gamma((Q^2 - 4)(1 - \omega_p^2)^2 + 2R^2)}{8(1 - \omega_p^2)^2} Q, \tag{24}$$

and

$$\frac{\partial \psi}{\partial T_1} = - \frac{m\omega_p^3}{2(1 - \omega_p^2)}. \tag{25}$$

We incorporate the conclusions (24) and (25) into Eq. (21), and obtain

$$\begin{aligned} & \frac{\partial^2 Z_1}{\partial T_0^2} + \omega_p^2 Z_1 - \frac{1}{4(1 - \omega_p^2)^3} \left(2\gamma(1 - \omega_p^2)^2 Q^2 R \right. \\ & \left. + \gamma(R^2 - 4(1 - \omega_p^2)^2) R + 8(1 - \omega_p^2)^2 \omega_p^2 \frac{\partial R}{\partial T_1} \right) \\ & \cos(T_0 + \phi) + \frac{2R\omega_p^2}{(1 - \omega_p^2)} \frac{\partial \phi}{\partial T_1} \sin(T_0 + \phi) \\ & - \frac{\gamma(2 + \omega_p) Q R^2}{4(1 - \omega_p^2)^2} \cos(2T_0 + \omega_p T_0 + 2\phi + \psi) \\ & + \frac{\gamma R^3}{4(1 - \omega_p^2)^3} \cos(3T_0 + 3\phi) \\ & + \frac{\gamma(2 - \omega_p) Q R^2}{4(1 - \omega_p^2)^2} \cos(2T_0 - \omega_p T_0 + 2\phi - \psi) \\ & - \frac{1}{4} \gamma \omega_p Q^3 \cos(3\omega_p T_0 + 3\psi) \\ & + \frac{\gamma(1 + 2\omega_p) Q^2 R}{4(1 - \omega_p^2)} \cos(T_0 + 2\omega_p T_0 + \phi + 2\psi) \\ & + \frac{\gamma(1 - 2\omega_p) Q^2 R}{4(1 - \omega_p^2)} \cos(T_0 - 2\omega_p T_0 + \phi - 2\psi) \\ & + \frac{\gamma(1 - 2\omega_p) Q^2 R}{4(1 - \omega_p^2)^2} \cos(T_0 - 2\omega_p T_0 + \phi - 2\psi) = 0. \end{aligned} \tag{26}$$

We can now solve Eq. (26) for Z_1 . The expression for Z_1 , being of minor interest, is provided in Appendix B. Proceeding further, we obtain the $\mathcal{O}(\mu^2)$ equations of the form

$$L_1 = 0 \quad \text{and} \quad L_2 = 0, \tag{27}$$

where L_1 and L_2 are long expressions also provided in [Appendix B](#). Eliminating secular terms from the equation $L_1 = 0$, we obtain

$$\frac{\partial R}{\partial T_2} = \left[-\frac{c}{2} - \frac{m\gamma \left(2(Q^2 - 2)(1 - \omega_p^2)^2 + R^2 \right)}{8(1 - \omega_p^2)^4} \right] R, \tag{28}$$

and

$$\frac{\partial \phi}{\partial T_2} = -\frac{m^2 \omega_p^4 (1 + 3\omega_p^2)}{8(1 - \omega_p^2)^3}. \tag{29}$$

Equation (28) governs the evolution of R . We incorporate Eqs. (28) and (29) into the equation $L_1 = 0$ and solve the resulting equation for X_2 . The expression for X_2 is provided in [Appendix B](#). We substitute the solution for X_2 into the equation $L_2 = 0$ and eliminate secular terms therein. We obtain

$$\begin{aligned} \frac{\partial Q}{\partial T_2} &= \left[\frac{m\gamma \omega_p^2 \left((Q^2 - 4)(2 - \omega_p^2)(1 - \omega_p^2)^2 + 2R^2(2 + \omega_p^2) \right)}{8(1 - \omega_p^2)^4} \right] Q, \end{aligned} \tag{30}$$

and

$$\begin{aligned} \frac{\partial \psi}{\partial T_2} &= -\frac{7\gamma^2}{256\omega_p} Q^4 + \frac{\gamma^2}{8\omega_p} (Q^2 - 1) \\ &+ \frac{\gamma^2(3\omega_p^2 - 2)}{64\omega_p(1 - \omega_p^2)^5} R^4 \\ &- \frac{\gamma^2(21\omega_p^4 - 14\omega_p^2 + 1)}{16\omega_p(1 - 9\omega_p^2)(1 - \omega_p^2)^3} Q^2 R^2 \\ &+ \frac{\gamma^2}{8\omega_p(1 - \omega_p^2)^2} R^2 + \frac{m^2 \omega_p^5 (\omega_p^2 + 3)}{8(1 - \omega_p^2)^3}. \end{aligned} \tag{31}$$

The fourth term on the right hand side of Eq. (31) indicates a 1:3 internal resonance, which we have avoided as our primary interest is in non-resonant interactions. As stated earlier, therefore, we simply assume $\omega_p \neq \frac{1}{3}$ in the present analysis.

4.3 Slow amplitude equations

We note that the evolution Eqs. (24), (28) and (30) for the amplitudes R and Q are independent of the phases ϕ and ψ . This is because the system is autonomous and

nonresonant. For stabilization of the block, the amplitudes R and Q are of primary interest. Therefore, we do not need the ϕ and ψ evolution Eqs. (18), (25), (29) and (31) any more.

Further, the evolution of Q given by Eq. (24) dominates while Eq. (30) provides only a tiny correction, because T_2 is a slower time scale than T_1 . Therefore, we may drop Eq. (30) while considering the evolution of Q . We are then left with two first-order equations, Eqs. (24) and (28). Recalling $T_1 = \mu t$ and $T_2 = \mu^2 t$ with $\mu = \sqrt{\varepsilon}$, we will work with

$$\frac{dQ}{dT_1} = -\frac{\gamma \left((Q^2 - 4)(1 - \omega_p^2)^2 + 2R^2 \right)}{8(1 - \omega_p^2)^2} Q + \mathcal{O}(\mu), \tag{32}$$

and

$$\frac{dR}{dT_1} = \mu \left[-\frac{c}{2} - \frac{m\gamma \left(2(Q^2 - 2)(1 - \omega_p^2)^2 + R^2 \right)}{8(1 - \omega_p^2)^4} \right] R. \tag{33}$$

Figure 2 compares two numerical solutions of Eqs. (6) and (7) with those of Eqs. (32) and (33). Although the primary system is negatively damped in both cases, with $c < 0$, Fig. 2a, b demonstrate suppression and growth, respectively. The match between the multiple scales solution (or slow amplitude equations) and full integration is seen to be very good. We now study the slow amplitude equations more systematically.

5 Canonical form

We now adopt a parameter-dependent transformation, including an $\mathcal{O}(1)$ stretching of the time T_1 , to simplify the slow flow Eqs. (32) and (33) into a unifying form. Writing $(1 - \omega_p^2)^2 = w$, we set

$$Q^2 = S \quad \text{and} \quad R^2 = wP \tag{34}$$

to obtain

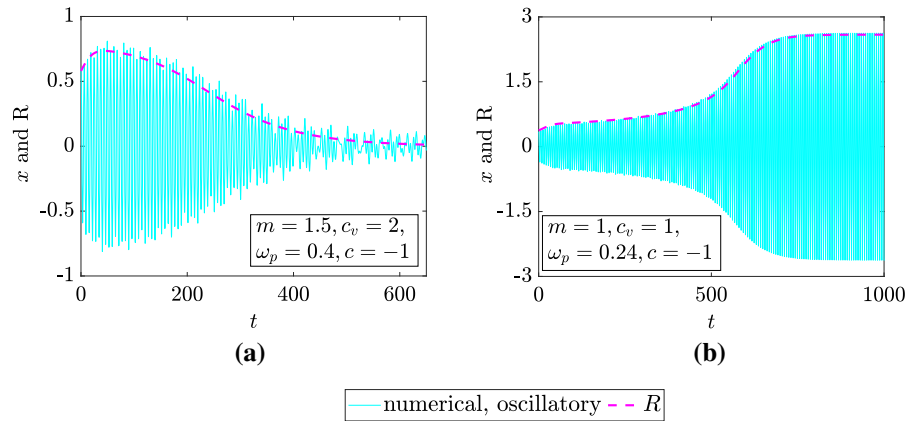
$$\frac{dS}{dT} = \mp (S + 2P - 4) S + \mathcal{O}(\bar{\mu}), \tag{35}$$

$$\frac{dP}{dT} = \mp \bar{\mu} (2S + P - 4 - c_1) P, \tag{36}$$

where

$$c_1 = -\frac{4cw}{m\gamma}, \quad \bar{\mu} = \frac{\mu m}{w}, \tag{37}$$

Fig. 2 Comparison of numerical solution of Eqs. (6) and (7) with that of Eqs. (32) and (33). $\varepsilon = 0.01$ in all cases. Subplots **a** and **b** demonstrate decaying and limit cycle solutions of the primary oscillator, respectively



and the T indicates that we have absorbed the $\mathcal{O}(1)$ factor of $\frac{|\gamma|}{4}$ into T_1 . The \mp sign reflects the sign of γ , with the negative being taken for $\gamma > 0$.

Based on the goals of this paper, we consider $\gamma > 0$, i.e., the negative sign in the \mp options above. It may be noted in Eq. (37) that our main interest is in $c < 0$ (primary system negatively damped) and $\gamma > 0$ (secondary system has a stable untuned limit cycle), and so we are mainly interested in $c_1 > 0$. However, from a dynamic systems viewpoint, if the primary system is changed to positively damped and the secondary system’s limit cycle oscillator also has its nonlinear damping reversed¹ then c_1 will remain unchanged while the positive sign will be adopted in the \mp options above, leading to the same phase portrait with flow directions reversed. With these observations, in what follows, we will take the negative sign in the \mp options above.

With the above motivation we finally write our main equations in canonical form, as obtained *via* the second-order multiple scales analysis:

$$\frac{dS}{dT} = -(S + 2P - 4)S + \mathcal{O}(\bar{\mu}), \tag{38}$$

$$\frac{dP}{dT} = -\bar{\mu}(2S + P - 4 - c_1)P, \tag{39}$$

with $0 < \bar{\mu} \ll 1$ and $c_1 > 0$. In the above, S and P correspond to the squares of the secondary and primary oscillators’ amplitudes, respectively.

Equations (38) and (39) are simpler than Eqs. (32) and (33). For $\bar{\mu}$ sufficiently small, the single physical parameter c_1 governs the qualitative dynamics of the

system. Interestingly, recalling $c_v = m\gamma$ from Eq. (5), we see that c_1 is superficially independent of the secondary oscillator’s mass m . Of course, the foregoing analysis assumes that there is indeed an $\mathcal{O}(1)$ mass m . The effect of m is retained in the frequency ω_p which in turn determines w .

6 Final slow amplitude dynamics

We now use Eqs. (38) and (39) to examine the dynamics on the first quadrant of the P - S plane. We first note that the S dynamics is typically much faster than the P dynamics. Accordingly, for the overall qualitative dynamics, we neglect the small $\mathcal{O}(\bar{\mu})$ term in Eq. (38), because retaining it would change the resulting phase portrait only slightly, at the cost of more complicated expressions and less clear insight. Comparisons with full numerical solutions of the original equations will support this simplification.

We also note that P and S axes form invariant manifolds: $S = 0$ yields dynamics purely on the P -axis, and vice versa.

On examining dynamics on the P -axis, by Eq. (39), we find an unstable point $P = 0$ and a stable point $P = 4 + c_1$. Further, by Eq. (38), it is easy to see that $S = 0$ is unstable for $P = 0$ and stable for $P = 4 + c_1$. Hence, the fixed points $(S = 0, P = 0)$ and $(0, 4 + c_1)$ are unstable and stable nodes, respectively.

Similarly, on the S -axis, by Eq. (38), we find an unstable fixed point $S = 0$ and a stable fixed point $S = 4$. By Eq. (39), for $S = 4$, stability of $P = 0$ requires $c_1 < 4$. Hence, the fixed point $(4, 0)$ is a stable node if $c_1 < 4$, and a saddle if $c_1 > 4$. Further, by Eqs. (38) and (39), the fourth and final fixed point is at the

¹ Upon changing the sign of γ , small solutions for that oscillator would be stable, large solutions would be unbounded, and there would be an unstable limit cycle.

intersection of the straight lines

$$S + 2P - 4 = 0, \quad \text{and} \quad 2S + P - 4 - c_1 = 0. \quad (40)$$

For $c_1 > 4$, the above lines do not intersect in the first quadrant. Therefore, the fourth fixed point exists for $0 < c_1 < 4$.

From the above, we conclude that the system dynamics has two qualitatively different regimes: $0 < c_1 < 4$ and $c_1 > 4$. The canonical form of our equations allows us to reach this far quite easily. We now study these two regimes separately.

6.1 Dynamics for $0 < c_1 < 4$

Recalling Eq. (40), the fourth fixed point named (S^*, P^*) is at

$$S^* = \frac{2}{3}(2 + c_1), \quad P^* = \frac{1}{3}(4 - c_1). \quad (41)$$

The stability of (S^*, P^*) is governed by the eigenvalues of a Jacobian matrix of the form

$$\mathbf{D} = \begin{bmatrix} -S^* + \mathcal{O}(\bar{\mu}) & -2S^* + \mathcal{O}(\bar{\mu}) \\ -2\bar{\mu}P^* & -\bar{\mu}(S^* - c_1) \end{bmatrix}, \quad (42)$$

where $\mathcal{O}(\bar{\mu})$ terms in the first row have been suppressed for simplicity. To obtain the eigenvalues of \mathbf{D} , we can solve the characteristic equation

$$\det(\mathbf{D} - \lambda \mathbf{I}) = 0.$$

But we can use asymptotic arguments to make progress through simpler expressions. The characteristic equation takes the form

$$(S^* + \lambda)\lambda + \mathcal{O}(\bar{\mu}) = 0. \quad (43)$$

Thus, one eigenvalue is

$$\lambda_1 = -S^* + \mathcal{O}(\bar{\mu})$$

and the other one is $\mathcal{O}(\bar{\mu})$. Consistent with these, we also note that $\text{tr}(\mathbf{D}) = -S^* + \mathcal{O}(\bar{\mu})$. The product of the eigenvalues is

$$\det(\mathbf{D}) = \bar{\mu}(S^* - c_1)S^* - 4\bar{\mu}P^*S^* + \mathcal{O}(\bar{\mu}^2).$$

Dropping the higher order small term and factoring out the known eigenvalue of $-S^*$, we find using Eq. (41) that the other eigenvalue is

$$\lambda_2 = -\bar{\mu}(S^* - 4P^* - c_1) = \bar{\mu}(4 - c_1) > 0$$

to leading order. Thus, the fixed point given by Eq. (41) is a saddle.

We next find the corresponding eigenvectors of λ_1 and λ_2 , given by

$$(\mathbf{D} - \lambda \mathbf{I})\mathbf{X} = \mathbf{0}, \quad (44)$$

where $\mathbf{X} = \{x_1, x_2\}^T$. For $\lambda = \lambda_1$, the second row in Eq. (44) yields

$$-2\bar{\mu}P^*x_1 - (\bar{\mu}(S^* - c_1) - S^*)x_2 = 0,$$

whence, x_2 is $\mathcal{O}(\bar{\mu})$. Hence, to $\mathcal{O}(1)$, the eigenvector corresponding to λ_1 is $\{1, 0\}^T$. For $\lambda = \lambda_2$, the second row in Eq. (44) yields

$$x_1 + 2x_2 = 0$$

at leading order, where we have substituted for P^* and S^* from Eq. (41). This means the eigenvector corresponding to λ_2 is $\{2, -1\}^T$. Graphically, the eigenvector corresponding to λ_1 (stable direction) is horizontal, and the eigenvector corresponding to λ_2 (unstable direction) is along a line like EF in Fig. 3a.

Fig. 3 Phase portraits for **a** $0 < c_1 < 4$ and **b** $c_1 > 4$. $\bar{\mu} = 0.05$ in both cases. Trajectories starting from different initial conditions are obtained by numerical integration of Eq. (39) along with Eq. (38) with the small $\mathcal{O}(\bar{\mu})$ term dropped

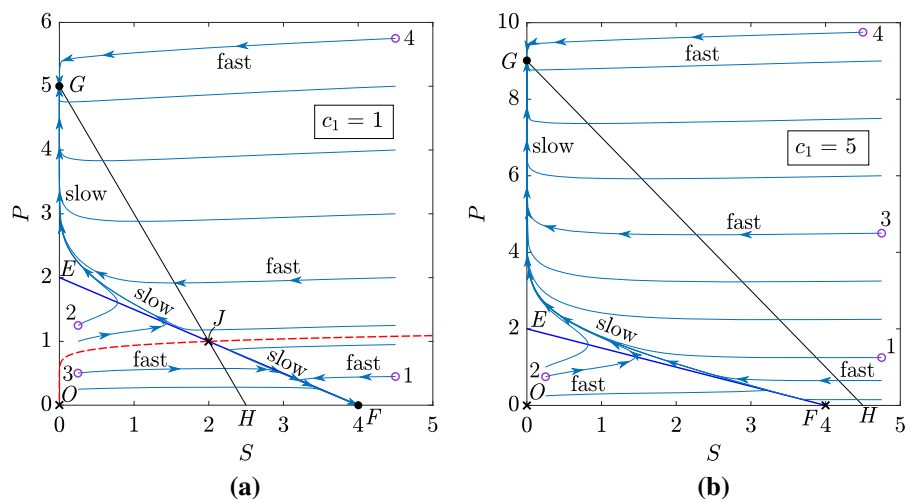


Figure 3a shows a phase portrait for $c_1 = 1$, which is representative of the case $0 < c_1 < 4$. The fixed points are: (i) $O(0, 0)$, unstable node, (ii) $F(4, 0)$, stable node, (iii) $G(0, 4 + c_1)$, stable node, and (iv) $J(S^*, P^*)$, saddle. Nearly-horizontal trajectories depict much faster evolution of S than P , as expected by the smallness of $\bar{\mu}$. Near the saddle, trajectories rapidly approach the unstable eigenvector and then turn to move more slowly and approximately along the unstable eigenvector direction, i.e., line EF . Trajectories toward F follow the line EF all the way, while trajectories towards E veer off to approach G on the vertical axis. The dashed (red) line is a separatrix that divides the plane into two regions: trajectories going to G and going to F . The separatrix was obtained numerically by reversing the flow from the saddle point with a tiny perturbation in the stable eigenvector direction, i.e., horizontal direction. This separatrix depicts the nature and extent of the vibration stabilization achieved. For initial conditions below the separatrix, the primary system is stabilized and the secondary system’s limit cycle is established. For initial conditions above the separatrix, the primary system wins the contest, the secondary system’s limit cycle is quenched, and the nonlinear damping of the secondary system serves to limit the oscillation amplitudes of the otherwise-linear primary system. As c_1 increases towards 4, the point H moves towards F , the separatrix moves downward, and the basin of attraction of the stabilized primary system shrinks in size. Recalling the definition of c_1 in Eq. (37), we see that c_1 is smaller if the negative damping level c of the primary system is smaller, if the strength of the van der Pol term γ is bigger, and if the untuned frequency ω_p of the secondary system is closer to unity. Note that with resonance at $\omega_p = 1$, the present analysis breaks down; ω_p should not be too close to unity for the stabilization strategy considered in this paper.

6.2 Dynamics for $c_1 > 4$

Figure 3b shows a phase portrait for $c_1 = 5$. The fixed points are: (i) $O(0, 0)$, unstable node, (ii) $F(4, 0)$, saddle, and (iii) $G(0, 4 + c_1)$, stable node. The intersection point J of the foregoing case has disappeared. The basin of attraction of stabilized motions of the primary system has shrunk to zero and then disappeared. Essentially all trajectories go to node G . As discussed above, the value of c_1 can be made smaller by increasing γ or

letting ω_p be closer to unity, but the upper limit of the present stabilization strategy, asymptotically for small μ , is analytically clear from the canonical equations: $c_1 = 4$.

We note that responses like in Fig. 3 are typical for systems with nonresonant double Hopf bifurcations: see [19,24–26] and also [27]. Therefore, Fig. 3 resembles some plots in these studies, e.g., see Fig. 4 in [19], Fig. 2 in [24], Fig. 2 in [25] and Fig. 5 in [26]. However, in contrast to those studies, in the present paper, we consider a specific parameter regime where one oscillator is much less massive than the other; where the secondary oscillator is destabilized with feedback to produce a limit cycle; and where the slow flow carried up to second-order is found to be such that everything can be expressed in terms of a single nondimensional parameter in canonical equations. In this way, our study makes significant new contributions although in a more narrow application area.

6.3 Parameter c_1 in terms of system parameters

We have observed that the nondimensional parameter c_1 governs the qualitative dynamics of the system. To reconnect with the original physical variables we note that, by Eqs. (3), (4), (5) and (37),

$$c_1 = -4 \frac{C}{\bar{c}_v} \left(1 - \frac{\omega^2}{\Omega^2} \right)^2, \tag{45}$$

where $C < 0$ and $\bar{c}_v > 0$ are in Eq. (1), and where Ω and ω are the natural frequencies of the primary and secondary oscillators, respectively. We recall the stabilization criterion $c_1 < 4$, and that lower c_1 gives a larger stabilization regime. Finally, we emphasize that $\omega \neq \Omega$ in our analysis. By Eq. (45), the following interpretations can now be made. Higher values of $\omega < \Omega$ lower the demand on \bar{c}_v . For example, with $\omega \sim 0.4\Omega$, \bar{c}_v is required to be higher than $0.84^2 C \approx 0.7C$. In comparison, with $\omega \sim 0.85\Omega$, \bar{c}_v is required to be higher than merely $0.077C$. Conversely, with the same \bar{c}_v , relatively larger ω can help to stabilize larger negative damping C . Always, by selecting high enough \bar{c}_v , we can achieve $c_1 < 4$, i.e.,

$$-\frac{C}{\bar{c}_v} \left(1 - \frac{\omega^2}{\Omega^2} \right)^2 < 1. \tag{46}$$

However, as emphasized repeatedly in this paper, precise near-resonant tuning ($\omega \approx \Omega$) is assumed to be absent. This allows the same stabilization system to continue working even under a change in operating parameters that changes Ω .

We next discuss system responses in terms of the original variables. In particular, we will demonstrate that widely different sets of parameter values corresponding to the same c_1 and $\bar{\mu}$ follow the same phase portrait.

6.4 Responses in terms of original variables

Recalling the transformations to variables P and S adopted in Eq. (34) from the amplitude variables Q and R introduced within the multiple scales analysis, we now present numerical solutions of the original Eqs. (6) and (7) and the slow amplitude Eqs. (32) and (33) in Figs. 4, 5, 6 and 7. These numerical solutions show an excellent qualitative match between the $\mathcal{O}(1)$ dynamics and the full numerical solutions; and they also show a small mismatch (as expected) when the leading order term in the solution goes to zero, because the next term in the expansion still remains nonzero. For a sizeable range of parameter values, in particular, it will be seen that the phase portraits obtained from the canonical equations yield accurate and useful insight into the dynamics of the original system.

These four Figs. 4, 5, 6 and 7 are arranged as follows. In each figure, the two subplots on the left correspond to a single set of parameter values corresponding to particular values of c_1 and $\bar{\mu}$, as well as one set of initial conditions; and the two subplots on the right correspond to a different set of parameter values corresponding to the *same* values of c_1 and $\bar{\mu}$, along with a different set of initial conditions. The upper subplots show the numerical solution for x , whose slowly varying amplitude is to be compared with the variable R ; and the lower subplots show the numerically obtained values of $z + \frac{x}{1 - \omega_p^2}$, whose slowly varying amplitude is to be compared with Q . In this way, the direct correspondence between the original oscillatory solutions and the slow amplitude solutions can be easily seen. The unifying role of the canonical equations is demonstrated as well. Individual details for the different figures, including initial conditions, are provided below.

Initial conditions in Fig. 4a, b respectively correspond to the points marked 1 and 2 in Fig. 3a. Figure 3a shows that the trajectory from initial condition 1 moves to the point $F(4, 0)$. The corresponding response in Fig. 4a shows that the primary system amplitude decays to a small value (upper plot), and the secondary system settles to a limit cycle with amplitude 2 (lower plot).

For the trajectory from initial condition 2 in Fig. 3a, S initially grows up to about 0.77 and then decays. The corresponding response in Fig. 4b initially grows to about $\sqrt{0.77} = 0.88$ and then decays (recall that $Q = \sqrt{S}$, Eq. (34)). In this solution the limit cycle of the secondary oscillator is quenched. The upper plot confirms the predicted steady nonzero oscillation of the primary system.

Next, see Fig. 5. Initial conditions in Fig. 5a, b correspond to the points marked 3 and 4 respectively in Fig. 3a. In Fig. 3a, for the trajectory from initial condition 3, P decays and S shows rapid initial growth followed by a slower increase. Figure 5a, on the left, shows the corresponding responses in the original variables. The upper subplot shows the decaying response of the primary system. In the lower subplot we see the fast initial growth in the secondary system's response followed by a slow approach to amplitude 2.

The trajectory from initial condition 4, in Fig. 3a, goes to $G(0, 5)$ with a rapid decay in S . Correspondingly in Fig. 5b, the upper subplot shows a steady oscillation while the lower subplot shows a rapid decay in amplitude. The secondary system's limit cycle is quenched for this initial condition, although the parameters are the same.

Similarly, consider Figs. 6 and 7. In these figures, $\varepsilon = 0.002$, $c_1 = 5$, and $\bar{\mu} = 0.05$. The initial conditions for Figs. 6a, b and 7a, b correspond to the points 1, 2, 3 and 4 respectively in Fig. 3b. In the upper subplots of these two figures, we observe that the primary system stabilizes to a limit cycle because all trajectories in Fig. 3b finally merge to $G(0, 9)$. The limit cycle amplitude is $3(1 - \omega_p^2)$ in these figures. The decay in the secondary oscillator's response is consistent with the corresponding trajectories in Fig. 3b. In particular, the relatively lower frequency (ω_p) of oscillations in the decaying portions of the lower subplots may be noted: after the decay is complete, the remaining oscillations are at the frequency of the primary oscillator, which is itself seen in the upper subplots.

For the trajectory from initial condition 1, the slow decay of S in Fig. 3b correlates with the secondary

Fig. 4 Numerical solutions of Eqs. (6) and (7) and Eqs. (32) and (33). For upper (respectively, lower) subplots, the dashed magenta line shows solutions for R (respectively, Q). For left and right subplots, initial conditions match points 1 and 2 respectively in Fig. 3a. $\varepsilon = 0.002$, $c_1 = 1$ and $\bar{\mu} = 0.05$ in all cases

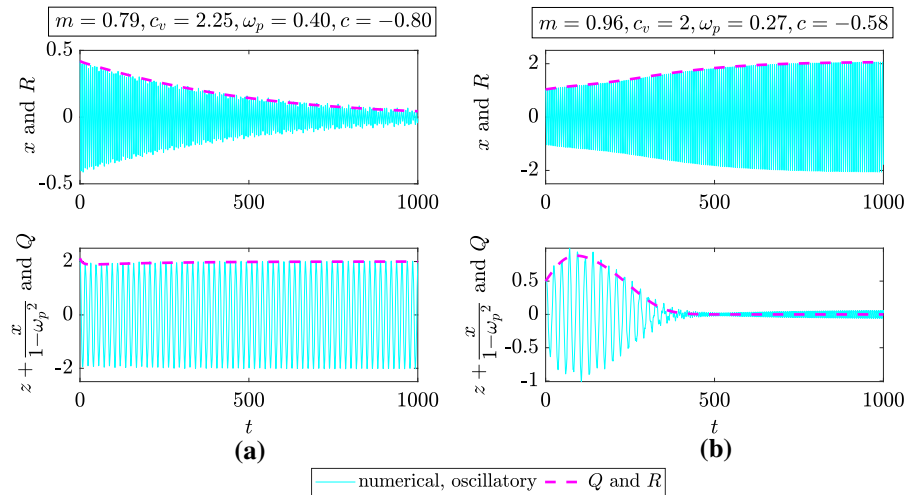


Fig. 5 Numerical solutions of Eqs. (6), (7), (32) and (33). For upper (respectively, lower) subplots, the dashed magenta line shows solutions for R (respectively, Q). For left and right subplots, initial conditions match points 3 and 4 respectively in Fig. 3a. $\varepsilon = 0.002$, $c_1 = 1$ and $\bar{\mu} = 0.05$ in all cases

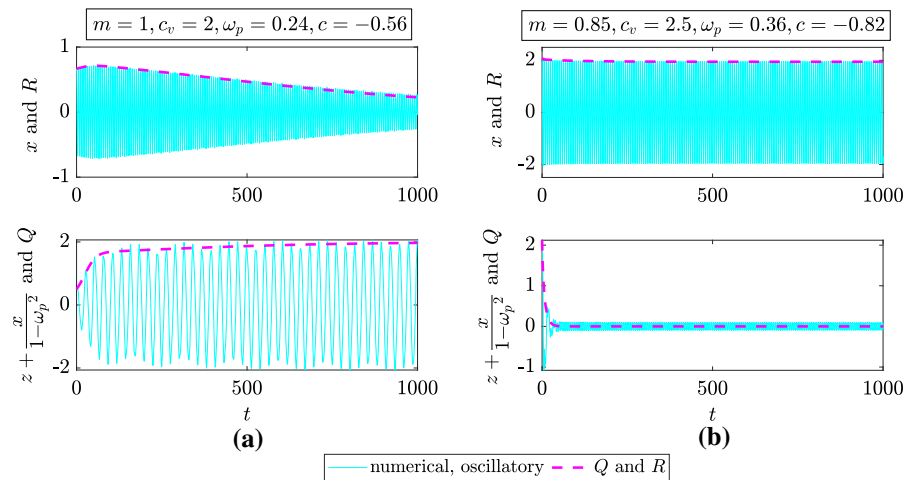


Fig. 6 Numerical solutions of Eqs. (6), (7), (32) and (33). For upper (respectively, lower) subplots, the dashed magenta line shows solutions for R (respectively, Q). For left and right subplots, initial conditions match points 1 and 2 respectively in Fig. 3b. $\varepsilon = 0.002$, $c_1 = 5$ and $\bar{\mu} = 0.05$ in all cases

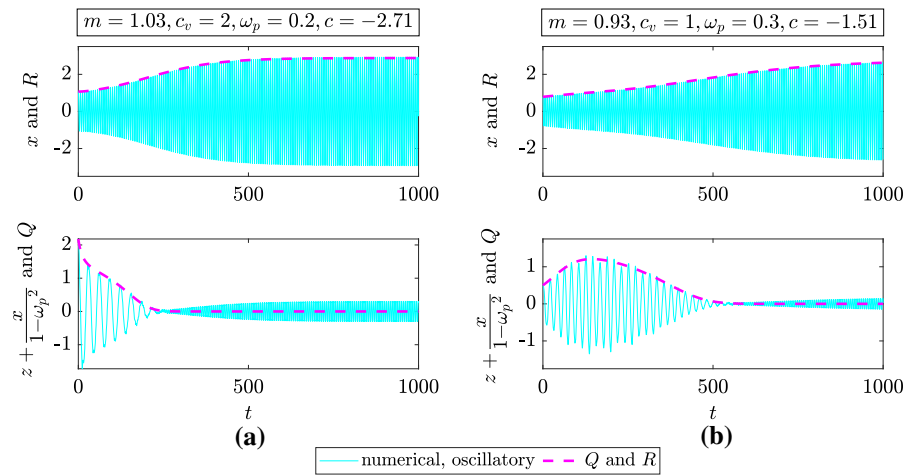
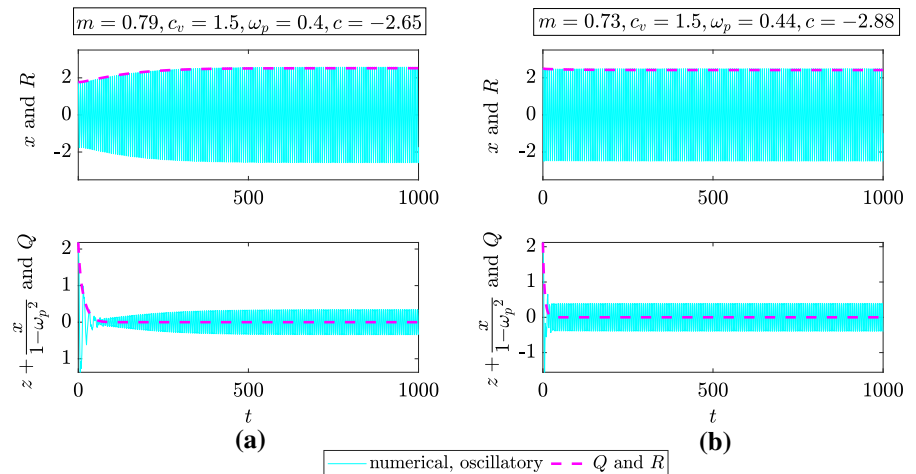


Fig. 7 Numerical solutions of Eqs. (6), (7), (32) and (33). For upper (respectively, lower) subplots, the dashed magenta line shows solutions for R (respectively, Q). For left and right subplots, initial conditions match points 3 and 4 respectively in Fig. 3b. $\varepsilon = 0.002$, $c_1 = 5$ and $\bar{\mu} = 0.05$ in all cases



oscillator's response in the lower plot of Fig. 6a. For the trajectory from initial condition 2, we notice that S initially grows up to about 1.46 and then decays. The lower plot in Fig. 6b confirms this increase-decrease evolution of the secondary oscillator's response. Further, for trajectories from initial conditions 3 and 4 in Fig. 3b, we notice the rapid initial decay of S . The lower subplots in the corresponding Figs. 7a, b show rapid initial decay in the secondary oscillator's response. As mentioned above, the remaining oscillations in the lower subplots, most clearly seen in Fig. 7b, are due to $\mathcal{O}(\mu)$ terms in the multiple scales expansion that have not been incorporated in the plots: see the expression for Z_1 in Appendix B.

In this way, through Figs. 4, 5, 6 and 7, it is seen that the slow dynamics captured by the second-order multiple scales analysis does a good job of capturing the qualitative behavior of quenching of the primary oscillator's unstable vibrations. Moreover, the phase portraits obtained from our canonical equations (38) and (39) give a simple and clear picture of the separatrix that lies between persistence and quenching of the primary unstable mode.

We end this paper by recalling that the solutions for x and z have been assumed to be $\mathcal{O}(1)$ with respect to $0 < \varepsilon \ll 1$. Numerical solutions show that if initial conditions for x (the unstable primary mode) are taken large enough, then solutions to the original Eqs. (6) and (7) can be unbounded. Recalling that $\gamma = c_v/m$ in Eqs. (6) and (7), and using the parameters of Fig. 7a, we present two large- x solutions in Fig. 8. Such failure of a nonlinear stabilizer at large amplitudes of the primary unstable oscillator is not surprising: see, e.g., [16].

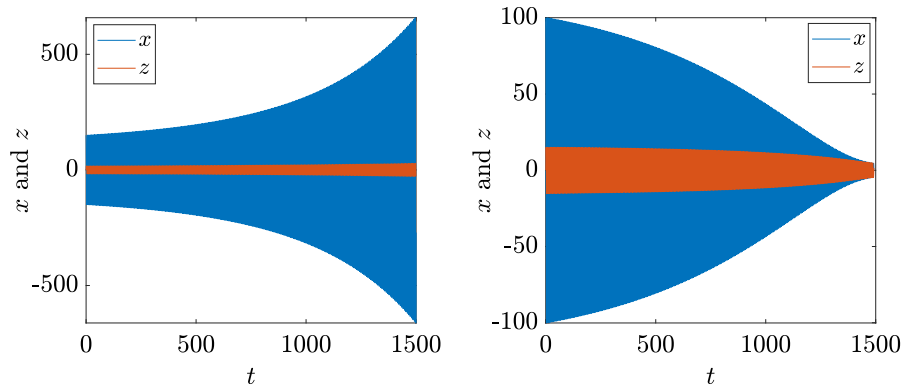
For such large-amplitude regimes the solution approach adopted in this paper, namely multiple scales based on treating x as $\mathcal{O}(1)$, is inappropriate. If such a regime is considered interesting, analysis using a different strategy may be undertaken in future work. For this paper, we simply note that extremely large amplitudes render our approximations invalid.

7 Conclusions

In this paper, we have studied the interaction between a weakly unstable and linear primary oscillator with an attached, small, secondary oscillator with its own non-resonant limit cycle. The practical motivation for studying such an untuned or nonresonant secondary oscillator is that precise tuning of physical parameters is no longer needed, and the stabilizer may remain effective even if system parameters drift to some extent.

The system studied is autonomous: there is no external forcing, and the goal is simply to render the primary mode of vibration stable. Since we have explicitly assumed there is no resonance, when we use the method of multiple scales and introduce amplitude and phase variables, a significant simplification occurs. The slow amplitude equations of the primary and secondary system decouple, and the phases of these two oscillators have no effect on the qualitative behavior of the system. The resulting two-dimensional phase portrait can be further simplified by a parameter-dependent change of variables which yields what we think is the simplest possible form for the slow flow, with one small perturbation parameter and only one $\mathcal{O}(1)$ system parame-

Fig. 8 Responses for large initial conditions for x . Parameters are the same as in Fig. 7a. Left: initial x -amplitude 150. Right: initial x -amplitude 100



ter, $c_1 > 0$. In particular, stabilization is possible for $c_1 < 4$. In the phase plane, the transformed coordinates lie in the first quadrant only. For $c_1 < 4$, a single separatrix divides the first quadrant into two regions. Solutions in one region display a quenching of the secondary oscillator's limit cycle along with a steady oscillation of the primary system. Solutions in the second region display a quenching of the unstable primary mode, along with a steady oscillation of the secondary system. As c_1 approaches 4, the second region shrinks in size and vanishes in the limit.

Future work may explore practical implementations of such a stabilizing device, as well as the possibility of stabilizing more than one unstable mode with a single additional oscillator. Note that if precise tuning of frequencies is needed, it is in general not possible to stabilize two modes of different frequencies using a single added stabilizing oscillator. In this way, we hope that our present analytical study of nonresonant modal interactions may lead to both new research as well as applications.

Author contributions **D. D. Tandel:** Detailed execution of analysis and writing. **Pankaj Wahi:** Conception, aspects of analysis and writing. **Anindya Chatterjee:** Conception, guidance and writing.

Funding We have not received any financial support for conducting this research.

Data Availability Not applicable.

Declarations

Competing interests The authors declare that they have no conflict of interest.

Appendix A Broader literature review

We have conducted a broader literature search and found 40 papers, of which 39 of them were published between 1980 and 2022. These papers each have the van der Pol oscillator coupled to either the van der Pol oscillator or some other oscillator. These papers are included in this article as references [20, 24, 25, 28–64]. These references can be grouped in various ways depending on which aspect of their contribution we wish to focus on. Each such grouping serves to emphasize how our work is different.

Many of these papers involve two coupled oscillators that are resonant, i.e., the natural frequencies are close. From our 40 references, it turns out that references [20, 28–46] are in this first category. Since our two oscillators have frequencies that are *not close*, we do not fall in this category of *resonant* coupled oscillators.

Another way to classify the papers is to identify those (27 out of 40) where the two oscillators' inertia terms are of equal or nearly equal magnitude, and their coupled dynamics, which may be weakly or strongly nonlinear, are then examined. References [24, 25, 28–42, 46–55] fall in this category. We do not fall in this category because our motivation is an *untuned vibration stabilizer* where the added system is necessarily small compared to the primary system, and it still affects the dynamics.

Another way to group some papers is to note those wherein two oscillators, by *mathematical design*, are capable of having perfectly synchronized solutions. In abstract first-order form, if we have

$$\dot{x} = f(x) + g(x, y) \quad \text{and} \quad \dot{y} = f(y) + g(y, x),$$

then $x = y$ is a possible solution satisfying

$$\dot{x} = f(x) + g(x, x).$$

Whether that phase-locked solution is stable or not then becomes important. If it is stable, the basin of attraction is important, and so on. Out of the 40, 9 papers fall in this category [29, 31–33, 36, 38, 39, 42, 46]. Since our two oscillators do not have this form, our paper does not fall into this category.

Then there are coupled van der Pol and Duffing systems, for which some papers study the dynamics near 1:1 resonance [41, 44, 49, 56, 57], phase-locked motions [49, 54], or assume comparable inertia [25, 41, 42, 49, 52–54]. As explained above, our paper is very different from these papers.

There are also studies of coupled van der Pol and Duffing systems that involve 1:2 or 1:3 resonances: see [58–61]. We focus on *nonresonant* interactions and so we do not fall in this category.

We note that nonresonant interactions were studied in [51–53], but there the inertias of the two oscillators were the same (as noted above), and they reported decoupled amplitude dynamics of the coupled oscillators, while our results with disparate inertias show a potentially useful coupled dynamics. Therefore we differ from those papers.

Finally, for parameter values that are not small and where analytical progress was limited, numerical or experimental approaches have been used [47, 50, 54, 62–64] to observe nonlinear responses like multistability and chaotic solutions. Our paper is not in this category.

In this way, there is at least one key difference, and usually more than one key difference, between our paper and these 40 papers.

Appendix B Expressions from multiple scale analysis

The solution for Z_1 is

$$\begin{aligned} Z_1(T_0, T_1, T_2) = & -\frac{1}{4(1 - \omega_p^2)^4} \\ & ((2\gamma\omega_p^4 - 4\gamma\omega_p^2 + 2\gamma)RQ^2 - (4\gamma\omega_p^4 - 8\gamma\omega_p^2 \\ & + 4\gamma - \gamma R^2)R) \cos(T_0 + \phi) + \frac{m\omega_p^4 R}{(1 - \omega_p^2)^3} \\ & \sin(T_0 + \phi) + \frac{\gamma R^3}{4(9 - \omega_p^2)(1 - \omega_p^2)^3} \cos(3T_0 + 3\phi) \end{aligned}$$

$$\begin{aligned} & -\frac{\gamma Q^3}{32\omega_p} \cos(3\omega_p T_0 + 3\psi) \\ & + \frac{(1 - 2\omega_p)\gamma Q^2 R}{4(1 - 3\omega_p)(1 + \omega_p)(1 - \omega_p)^2} \\ & \cos(T_0 - 2\omega_p T_0 + \phi - 2\psi) \\ & + \frac{(1 + 2\omega_p)\gamma Q^2 R}{4(1 + 3\omega_p)(1 - \omega_p)(1 + \omega_p)^2} \\ & \cos(T_0 + 2\omega_p T_0 + \phi + 2\psi) \\ & + \frac{\gamma(2 - \omega_p)QR^2}{16(1 - \omega_p)(1 - \omega_p^2)^2} \\ & \cos(2T_0 - \omega_p T_0 + 2\phi - \psi) \\ & - \frac{\gamma(2 + \omega_p)QR^2}{16(1 + \omega_p)(1 - \omega_p^2)^2} \\ & \cos(2T_0 + \omega_p T_0 + 2\phi + \psi). \end{aligned} \tag{B.1}$$

Recall Eq. (27), the expressions are

$$\begin{aligned} L_1 = & \frac{\partial^2 X_2}{\partial T_0^2} + X_2 - \left(\frac{m^2 \omega_p^4 (1 + 3\omega_p^2) R}{4(1 - \omega_p^2)^3} \right. \\ & \left. + 2R \frac{\partial \phi}{\partial T_2} \right) \sin(T_0 + \phi) \\ & + \left(cR + \frac{m\gamma (2(Q^2 - 2)(1 - \omega_p^2)^2 + R^2) R}{4(1 - \omega_p^2)^4} \right. \\ & \left. + 2 \frac{\partial R}{\partial T_2} \right) \cos(T_0 + \phi) \\ & - \frac{m\gamma \omega_p ((Q^2 - 4)(1 - \omega_p^2)^2 + 2R^2) Q}{4(1 - \omega_p^2)^3} \\ & \cos(\omega_p T_0 + \psi) \\ & + \frac{m^2 \omega_p^6 Q}{(1 - \omega_p^2)^2} \sin(\omega_p T_0 + \psi) + \frac{9m\gamma \omega_p Q^3}{32} \\ & \cos(3\omega_p T_0 + 3\psi) \\ & - \frac{9m\gamma R^3}{4(9 - \omega_p^2)(1 - \omega_p^2)^3} \cos(3T_0 + 3\phi) \\ & - \frac{m\gamma(1 + 2\omega_p)^3 Q^2 R}{4(1 + 3\omega_p)(1 - \omega_p)(1 + \omega_p)^2} \\ & \cos(T_0 + 2\omega_p T_0 + \phi + 2\psi) \\ & - \frac{m\gamma(1 - 2\omega_p)^3 Q^2 R}{4(1 - 3\omega_p)(1 + \omega_p)(1 - \omega_p)^2} \\ & \cos(T_0 - 2\omega_p T_0 + \phi - 2\psi) \\ & + \frac{m\gamma(2 + \omega_p)^3 QR^2}{16(1 + \omega_p)(1 - \omega_p^2)^2} \\ & \cos(2T_0 + \omega_p T_0 + 2\phi + \psi) \\ & - \frac{m\gamma(2 - \omega_p)^3 QR^2}{16(1 - \omega_p)(1 - \omega_p^2)^2} \\ & \cos(2T_0 - \omega_p T_0 + 2\phi - \psi), \end{aligned} \tag{B.2}$$

and

$$\begin{aligned}
 L_2 = & \frac{\partial^2 Z_2}{\partial T_0^2} + \omega_p^2 Z_2 + \frac{\partial^2 X_2}{\partial T_0^2} \\
 & + \frac{\omega_p^2}{8(1 - \omega_p^2)^5} \left(m\gamma(6\omega_p^6 - 10\omega_p^4 + 2\omega_p^2 \right. \\
 & + 2)Q^2 R + m\gamma(-12\omega_p^6 + 20\omega_p^4 - 4\omega_p^2 \\
 & - 4 + 7\omega_p^2 R^2 + R^2)R + (-16\omega_p^8 + 64\omega_p^6 \\
 & - 96\omega_p^4 + 64\omega_p^2 - 16) \frac{\partial R}{\partial T_2} \left. \right) \cos(T_0 + \phi) \\
 & + \frac{1}{16(9 - \omega_p^2)(1 - 9\omega_p^2)(1 - \omega_p^2)^6} \\
 & \left((-45\omega_p^{10} + 518\omega_p^8 - 1110\omega_p^6 + 864\omega_p^4 \right. \\
 & - 245\omega_p^2 + 18)\gamma^2 R^2 Q^2 + (-18\omega_p^{14} \\
 & + 264\omega_p^{12} - 1150\omega_p^{10} + 2356\omega_p^8 \\
 & - 2574\omega_p^6 + 1504\omega_p^4 - 418\omega_p^2 + 36)\gamma^2 Q^4 \\
 & + (18\omega_p^4 - 92\omega_p^2 + 10)\gamma^2 R^4 \\
 & + (72\omega_p^{14} - 1016\omega_p^{12} + 4072\omega_p^{10} \\
 & - 7640\omega_p^8 + 7640\omega_p^6 \\
 & - 4072\omega_p^4 + 1016\omega_p^2 - 72)\gamma^2 Q^2 \\
 & + (-72\omega_p^8 + 800\omega_p^6 - 1456\omega_p^4 \\
 & + 800\omega_p^2 - 72)\gamma^2 R^2 \\
 & + m^2(-36\omega_p^{16} + 292\omega_p^{14} + 472\omega_p^{12} \\
 & - 1784\omega_p^{10} + 1164\omega_p^8 - 108\omega_p^6) + \gamma^2(144\omega_p^{12} \\
 & - 1888\omega_p^{10} + 6256\omega_p^8 - 9024\omega_p^6 \\
 & + 6256\omega_p^4 - 1888\omega_p^2 + 144) + (-288\omega_p^{16} \\
 & + 4064\omega_p^{14} - 16288\omega_p^{12} \\
 & + 30560\omega_p^{10} - 30560\omega_p^8 + 16288\omega_p^6 - 4064\omega_p^4 \\
 & + 288\omega_p^2) \frac{\partial \phi}{\partial T_2} \left. \right) R \sin(T_0 + \phi) + \frac{\omega_p}{4(1 - \omega_p^2)^4} \\
 & \left((\omega_p^8 - 3\omega_p^6 + 3\omega_p^4 - \omega_p^2)m\gamma Q^3 \right. \\
 & + (-2\omega_p^4 - 2\omega_p^2)m\gamma R^2 Q + (-4\omega_p^8 + 12\omega_p^6 \\
 & - 12\omega_p^4 + 4\omega_p^2)m\gamma Q + (8\omega_p^8 - 32\omega_p^6 \\
 & + 48\omega_p^4 - 32\omega_p^2 + 8) \frac{\partial Q}{\partial T_2} \left. \right) \cos(\omega_p T_0 + \psi) \\
 & - \frac{1}{128(1 - 9\omega_p^2)(1 - \omega_p^2)^5} \left((336\omega_p^8 \right. \\
 & - 896\omega_p^6 + 800\omega_p^4 - 256\omega_p^2 + 16)\gamma^2 R^2 Q^2 \\
 & + (63\omega_p^{12} - 322\omega_p^{10} + 665\omega_p^8 - 700\omega_p^6 \\
 & + 385\omega_p^4 - 98\omega_p^2 + 7)\gamma^2 Q^4 \\
 & + (108\omega_p^4 - 84\omega_p^2 + 8)\gamma^2 R^4 \\
 & + (-288\omega_p^{12} + 1472\omega_p^{10} - 3040\omega_p^8 + 3200\omega_p^6 \\
 & - 1760\omega_p^4 + 448\omega_p^2 - 32)\gamma^2 Q^2
 \end{aligned}$$

$$\begin{aligned}
 & + (-288\omega_p^8 + 896\omega_p^6 - 960\omega_p^4 \\
 & + 384\omega_p^2 - 32)\gamma^2 R^2 \\
 & + m^2(-864\omega_p^{14} + 2688\omega_p^{12} - 2880\omega_p^{10} \\
 & + 1152\omega_p^8 - 96\omega_p^6) \\
 & + \gamma^2(288\omega_p^{12} - 1472\omega_p^{10} + 3040\omega_p^8 \\
 & - 3200\omega_p^6 + 1760\omega_p^4 - 448\omega_p^2 + 32) \\
 & + (2304\omega_p^{13} - 11776\omega_p^{11} + 24320\omega_p^9 \\
 & - 25600\omega_p^7 + 14080\omega_p^5 - 3584\omega_p^3 \\
 & + 256\omega_p) \frac{\partial \psi}{\partial T_2} \left. \right) Q \sin(\omega_p T_0 + \psi) \\
 & + \frac{m\gamma\omega_p^2(7\omega_p^4 - 46\omega_p^2 - 9)R^3}{8(9 - \omega_p^2)(1 - \omega_p^2)^5} \cos(3T_0 + 3\phi) \\
 & - \frac{3\gamma^2 R^3}{16(9 - \omega_p^2)(1 - \omega_p^2)^6} \left((\omega_p^8 - 17\omega_p^6 + 69\omega_p^4 \right. \\
 & - 91\omega_p^2 + 38)Q^2 + (-3\omega_p^2 + 11)R^2 + 8\omega_p^6 \\
 & - 56\omega_p^4 + 88\omega_p^2 - 40) \sin(3T_0 + 3\phi) - \frac{5m\gamma\omega_p^3 Q^3}{32(1 - \omega_p^2)} \\
 & \cos(3\omega_p T_0 + 3\psi) + \frac{\gamma^2 Q^3}{128(1 - 9\omega_p^2)(1 - \omega_p^2)^3} \\
 & \left((9\omega_p^8 - 28\omega_p^6 + 30\omega_p^4 - 12\omega_p^2 + 1)Q^2 \right. \\
 & + (540\omega_p^4 - 152\omega_p^2 - 4)R^2 + 72\omega_p^8 \\
 & - 224\omega_p^6 + 240\omega_p^4 - 96\omega_p^2 + 8) \sin(3\omega_p T_0 + 3\psi) \\
 & + \frac{5\gamma^2 R^5}{16(9 - \omega_p^2)(1 - \omega_p^2)^5} \sin(5T_0 + 5\phi) \\
 & - \frac{5\gamma^2 Q^5}{128} \sin(5\omega_p T_0 + 5\psi) \\
 & - \frac{m\gamma\omega_p^2(22\omega_p^4 + 3\omega_p^3 - 3\omega_p^2 + \omega_p + 1)RQ^2}{8(1 + 3\omega_p)(1 - \omega_p^2)^3} \\
 & \cos(T_0 + 2\omega_p T_0 + \phi + 2\psi) \\
 & - \frac{m\gamma\omega_p^2(22\omega_p^4 - 3\omega_p^3 - 3\omega_p^2 - \omega_p + 1)RQ^2}{8(1 - 3\omega_p)(1 - \omega_p^2)^3} \\
 & \cos(T_0 - 2\omega_p T_0 + \phi - 2\psi) \\
 & + \frac{m\gamma\omega_p^2(\omega_p^4 + 7\omega_p^3 + 14\omega_p^2 - 2\omega_p + 4)QR^2}{16(1 - \omega_p^2)^4} \\
 & \cos(2T_0 + \omega_p T_0 + 2\phi + \psi) \\
 & - \frac{m\gamma\omega_p^2(\omega_p^4 - 7\omega_p^3 + 14\omega_p^2 + 2\omega_p + 4)QR^2}{16(1 - \omega_p^2)^4} \\
 & \cos(2T_0 - \omega_p T_0 + 2\phi - \psi) \\
 & + \frac{\gamma^2(4 + \omega_p)(\omega_p^3 + 2\omega_p^2 - 17\omega_p - 26)QR^4}{64(9 - \omega_p^2)(1 + \omega_p)(1 - \omega_p^2)^4} \\
 & \sin(4T_0 + \omega_p T_0 + 4\phi + \psi) \\
 & + \frac{\gamma^2(4 - \omega_p)(\omega_p^3 - 2\omega_p^2 - 17\omega_p + 26)QR^4}{64(9 - \omega_p^2)(1 - \omega_p)(1 - \omega_p^2)^4} \\
 & \sin(4T_0 - \omega_p T_0 + 4\phi - \psi)
 \end{aligned}$$

$$\begin{aligned}
 & + \frac{\gamma^2(1+4\omega_p)(11\omega_p^2+8\omega_p+1)Q^4R}{64\omega_p(1+3\omega_p)(1+\omega_p)(1-\omega_p^2)} \\
 & \sin(T_0+4\omega_pT_0+\phi+4\psi) \\
 & - \frac{\gamma^2(1-4\omega_p)(11\omega_p^2-8\omega_p+1)Q^4R}{64\omega_p(1-3\omega_p)(1-\omega_p)(1-\omega_p^2)} \\
 & \sin(T_0-4\omega_pT_0+\phi-4\psi) \\
 & + \frac{\gamma^2RQ^2}{64\omega_p(1-9\omega_p^2)(1-\omega_p^2)^3} \\
 & \left((5\omega_p^2+54\omega_p^7+135\omega_p^6-186\omega_p^5-141\omega_p^4 \right. \\
 & +146\omega_p^3-14\omega_p+1)Q^2+(-36\omega_p^4+78\omega_p^3 \\
 & -2\omega_p^2-4\omega_p)R^2+48\omega_p^7-32\omega_p^2 \\
 & -224\omega_p^6+112\omega_p^5+256\omega_p^4-176\omega_p^3+16\omega_p) \\
 & \left. \sin(T_0-2\omega_pT_0+\phi-2\psi) \right) \\
 & + \frac{\gamma^2RQ^2}{64\omega_p(1-9\omega_p^2)(1-\omega_p^2)^3} \\
 & \left((-5\omega_p^2+54\omega_p^7-135\omega_p^6-186\omega_p^5+141\omega_p^4 \right. \\
 & +146\omega_p^3-14\omega_p-1)Q^2+(36\omega_p^4+78\omega_p^3 \\
 & +2\omega_p^2-4\omega_p)R^2+48\omega_p^7+224\omega_p^6 \\
 & +112\omega_p^5-256\omega_p^4-176\omega_p^3+32\omega_p^2+16\omega_p) \\
 & \left. \sin(T_0+2\omega_pT_0+\phi+2\psi) \right) \\
 & - \frac{\gamma^2QR^2}{32(1-3\omega_p)(9-\omega_p^2)(1-\omega_p^2)^5} \\
 & \left((3\omega_p^{10}-18\omega_p^9-48\omega_p^8+283\omega_p^7 \right. \\
 & +193\omega_p^6-1277\omega_p^5+7\omega_p^4+1777\omega_p^3 \\
 & -416\omega_p^2-765\omega_p+261)Q^2 \\
 & +(-6\omega_p^5-22\omega_p^4+116\omega_p^3+84\omega_p^2 \\
 & -334\omega_p+98)R^2+12\omega_p^9+44\omega_p^8-256\omega_p^7 \\
 & -448\omega_p^6+1592\omega_p^5+440\omega_p^4-2464\omega_p^3 \\
 & +288\omega_p^2+1116\omega_p-324) \\
 & \left. \sin(2T_0-\omega_pT_0+2\phi-\psi) \right) \\
 & + \frac{\gamma^2QR^2}{32(1+3\omega_p)(9-\omega_p^2)(1-\omega_p^2)^5} \\
 & \left((3\omega_p^{10}+18\omega_p^9-48\omega_p^8-283\omega_p^7+193\omega_p^6 \right. \\
 & +1277\omega_p^5+7\omega_p^4-1777\omega_p^3-416\omega_p^2+765\omega_p \\
 & +261)Q^2+(6\omega_p^5-22\omega_p^4-116\omega_p^3+84\omega_p^2 \\
 & +334\omega_p+98)R^2-12\omega_p^9+44\omega_p^8+256\omega_p^7 \\
 & -448\omega_p^6-1592\omega_p^5+440\omega_p^4 \\
 & +2464\omega_p^3+288\omega_p^2-1116\omega_p-324) \\
 & \left. \sin(2T_0+\omega_pT_0+2\phi+\psi) \right) \\
 & - \frac{\gamma^2(2+3\omega_p)(6\omega_p^3+49\omega_p^2+24\omega_p+1)R^2Q^3}{128\omega_p(1+3\omega_p)(1+\omega_p)(1-\omega_p^2)^2} \\
 & \sin(2T_0+3\omega_pT_0+2\phi+3\psi)
 \end{aligned}$$

$$\begin{aligned}
 & + \frac{\gamma^2(2-3\omega_p)(6\omega_p^3-49\omega_p^2+24\omega_p-1)R^2Q^3}{128\omega_p(1-3\omega_p)(1-\omega_p)(1-\omega_p^2)^2} \\
 & \sin(2T_0-3\omega_pT_0+2\phi-3\psi) \\
 & - \frac{\gamma^2(3+2\omega_p)(3\omega_p^4+11\omega_p^3-29\omega_p^2-107\omega_p-38)R^3Q^2}{32(1+3\omega_p)(9-\omega_p^2)(1+\omega_p)(1-\omega_p^2)^3} \\
 & \sin(3T_0+2\omega_pT_0 \\
 & +3\phi+2\psi) \\
 & - \frac{\gamma^2(3-2\omega_p)(3\omega_p^4-11\omega_p^3-29\omega_p^2+107\omega_p-38)}{32(1-3\omega_p)(9-\omega_p^2)(1-\omega_p)(1-\omega_p^2)^3} \\
 & R^3Q^2\sin(3T_0-2\omega_pT_0+3\phi-2\psi).
 \end{aligned} \tag{B.3}$$

The solution for X_2 is

$$\begin{aligned}
 X_2(T_0, T_1, T_2) & = \frac{((Q^2-4)(1-\omega_p^2)^2+2R^2)m\gamma Q\omega_p}{4(1-\omega_p^2)^4} \\
 & \cos(\omega_pT_0+\psi) \\
 & - \frac{Qm^2\omega_p^6}{(1-\omega_p^2)^3} \sin(\omega_pT_0+\psi) \\
 & - \frac{9m\gamma\omega_pQ^3}{32(1-9\omega_p^2)} \cos(3\omega_pT_0+3\psi) \\
 & - \frac{9m\gamma R^3}{32(9-\omega_p^2)(1-\omega_p^2)^3} \cos(3T_0+3\phi) \\
 & - \frac{(1+2\omega_p)^3m\gamma RQ^2}{16\omega_p(1+3\omega_p)(1-\omega_p)(1+\omega_p)^3} \\
 & \cos(T_0+\phi+2\omega_pT_0+2\psi) \\
 & + \frac{(1-2\omega_p)^3m\gamma RQ^2}{16\omega_p(1-3\omega_p)(1+\omega_p)(1-\omega_p)^3} \\
 & \cos(T_0+\phi-2\omega_pT_0-2\psi) \\
 & + \frac{(2+\omega_p)^3m\gamma R^2Q}{16(3+\omega_p)(1-\omega_p)^2(1+\omega_p)^4} \\
 & \cos(2T_0+2\phi+\omega_pT_0+\psi) \\
 & - \frac{(2-\omega_p)^3m\gamma R^2Q}{16(3-\omega_p)(1+\omega_p)^2(1-\omega_p)^4} \\
 & \cos(2T_0+2\phi-\omega_pT_0-\psi)
 \end{aligned} \tag{B.4}$$

References

1. Frahm, H.: Device for damping vibrations of bodies. US Patent 989958 (1911)
2. Ibrahim, R.A.: Recent advances in nonlinear passive vibration isolators. *J. Sound Vib.* **314**(3–5), 371–452 (2008)
3. Ding, H., Chen, L.Q.: Designs, analysis, and applications of nonlinear energy sinks. *Nonlinear Dyn.* **100**, 3061–3107 (2020)
4. Gatti, G.: Fundamental insight on the performance of a nonlinear tuned mass damper. *Meccanica* **53**, 111–123 (2018)

5. Starosvetsky, Y., Gendelman, O.V.: Vibration absorption in systems with a nonlinear energy sink: Nonlinear damping. *J. Sound Vib.* **324**(3–5), 916–939 (2009)
6. Zhu, S.J., Zheng, Y.F., Fu, Y.M.: Analysis of non-linear dynamics of a two-degree-of-freedom vibration system with non-linear damping and non-linear spring. *J. Sound Vib.* **271**(1–2), 15–24 (2004)
7. Verhulst, F.: Quenching of self-excited vibrations. *J. Eng. Math.* **53**, 349–358 (2005)
8. Lee, Y.S., Vakakis, A.F., Bergman, L.A., McFarland, D.M.: Suppression of limit cycle oscillations in the van der Pol oscillator by means of passive non-linear energy sinks. *Struct. Control Health Monit.* **13**, 41–75 (2006)
9. Habib, G., Kerschen, G.: Suppression of limit cycle oscillations using the nonlinear tuned vibration absorber. *Proc. R. Soc. A Math. Phys. Eng. Sci.* **471**(2176), 20140976 (2015)
10. Wang, J.S., Fan, D., Lin, K.: A review on flow-induced vibration of offshore circular cylinders. *J. Hydrodyn.* **32**, 415–440 (2020)
11. Nasrabadi, M., Sevbitov, A.V., Maleki, V.A., Akbar, N., Javanshir, I.: Passive fluid-induced vibration control of viscoelastic cylinder using nonlinear energy sink. *Mar. Struct.* **81**, 103116 (2022)
12. Guo, H., Liu, B., Yu, Y., Cao, S., Chen, Y.: Galloping suppression of a suspended cable with wind loading by a nonlinear energy sink. *Arch. Appl. Mech.* **87**, 1007–1018 (2017)
13. Qin, Z., Chen, Y., Zhan, X., Liu, B., Zhu, K.: Research on the galloping and anti-galloping of the transmission line. *Int. J. Bifurc. Chaos* **22**(02), 1250038 (2012)
14. Dai, H.L., Abdelkefi, A., Wang, L.: Usefulness of passive non-linear energy sinks in controlling galloping vibrations. *Int. J. Non-Linear Mech.* **81**, 83–94 (2016)
15. Shirude, A., Vyasrayani, C.P., Chatterjee, A.: Towards design of a nonlinear vibration stabilizer for suppressing single-mode instability. *Nonlinear Dyn.* **103**, 1563–1583 (2021)
16. Singla, S., Chatterjee, A.: Nonlinear responses of an SDOF structure with a light, whirling, driven, untuned pendulum. *Int. J. Mech. Sci.* **168**, 105305 (2020)
17. Chatterjee, S.: On the efficacy of an active absorber with internal state feedback for controlling self-excited oscillations. *J. Sound Vib.* **330**(7), 1285–1299 (2011)
18. Mondal, J., Chatterjee, S.: Controlling self-excited vibration of a nonlinear beam by nonlinear resonant velocity feedback with time-delay. *Int. J. Non-Linear Mech.* **131**, 103684 (2021)
19. Gattulli, V., Di Fabio, F., Luongo, A.: Simple and double Hopf bifurcations in aeroelastic oscillators with tuned mass dampers. *J. Frankl. Inst.* **338**(2–3), 187–201 (2001)
20. Gattulli, V., Di Fabio, F., Luongo, A.: Nonlinear tuned mass damper for self-excited oscillations. *Wind Struct.* **7**(4), 251–264 (2004)
21. Nayfeh, A.H.: *Perturbation Methods*. Wiley, New York (2000)
22. Nayfeh, A.H., Mook, D.T.: *Nonlinear Oscillations*. Wiley, New York (1979)
23. Cartmell, M.P., Ziegler, S., Khanin, R., Forehand, D.: Multiple scales analyses of the dynamics of weakly nonlinear mechanical systems. *Appl. Mech. Rev.* **56**(5), 455–492 (2003)
24. Storti, D.W., Rand, R.H.: Dynamics of two strongly coupled van der Pol oscillators. *Int. J. Non-Linear Mech.* **17**(3), 143–152 (1982)
25. Natsiavas, S.: Free vibration of two coupled nonlinear oscillators. *Nonlinear Dyn.* **6**, 69–86 (1994)
26. Yamashita, K., Yagyu, T., Yabuno, H.: Nonlinear interactions between unstable oscillatory modes in a cantilevered pipe conveying fluid. *Nonlinear Dyn.* **98**, 2927–2938 (2019)
27. Guckenheimer, J., Holmes, P.: *Nonlinear Oscillations, Dynamical Systems, and Bifurcations of Vector Fields*. Springer-Verlag, New York (1983)
28. Rand, R.H., Holmes, P.J.: Bifurcation of periodic motions in two weakly coupled van der Pol oscillators. *Int. J. Non-Linear Mech.* **15**(4–5), 387–399 (1980)
29. Storti, D.W., Rand, R.H.: Dynamics of two strongly coupled relaxation oscillators. *SIAM J. Appl. Math.* **46**(1), 56–67 (1986)
30. Chakraborty, T., Rand, R.H.: The transition from phase locking to drift in a system of two weakly coupled van der Pol oscillators. *Int. J. Non-Linear Mech.* **23**(5–6), 369–376 (1988)
31. Storti, D.W., Reinhall, P.G.: Stability of in-phase and out-of-phase modes for a pair of linearly coupled van der Pol oscillators. In: Guran, A. (ed.) *Nonlinear Dynamics: The Richard Rand 50th Anniversary Volume*, pp. 1–23. World Scientific, Singapore (1997)
32. Storti, D.W., Reinhall, P.G.: Phase-locked mode stability for coupled van der Pol oscillators. *J. Vib. Acoust.* **122**(3), 318–323 (2000)
33. Wirkus, S., Rand, R.: The dynamics of two coupled van der Pol oscillators with delay coupling. *Nonlinear Dyn.* **30**, 205–221 (2002)
34. Low, L.A., Reinhall, P.G., Storti, D.W.: An investigation of coupled van der Pol oscillators. *J. Vib. Acoust.* **125**(2), 162–169 (2003)
35. Ivanchenko, M.V., Osipov, G.V., Shalfeev, V.D., Kurths, J.: Synchronization of two non-scalar-coupled limit-cycle oscillators. *Phys. D* **189**(1–2), 8–30 (2004)
36. Camacho, E., Rand, R., Howland, H.: Dynamics of two van der Pol oscillators coupled via a bath. *Int. J. Solids Struct.* **41**(8), 2133–2143 (2004)
37. Tang, J., Han, F., Xiao, H., Wu, X.: Amplitude control of a limit cycle in a coupled van der Pol system. *Nonlinear Anal. Theory Methods Appl.* **71**(7–8), 2491–2496 (2009)
38. Zhang, J., Gu, X.: Stability and bifurcation analysis in the delay-coupled van der Pol oscillators. *Appl. Math. Model.* **34**(9), 2291–2299 (2010)
39. Kulikov, D.A.: Dynamics of coupled van der Pol oscillators. *J. Math. Sci.* **262**, 817–824 (2022)
40. Poliashenko, M., McKay, S.R., Smith, C.W.: Hysteresis of synchronous-asynchronous regimes in a system of two coupled oscillators. *Phys. Rev. A* **43**(10), 5638–5641 (1991)
41. Chunbiao, G., Qishao, L., Kelei, H.: Strongly resonant bifurcations of nonlinearly coupled van der Pol-Duffing oscillator. *Appl. Math. Mech.* **20**, 68–75 (1999)
42. Zang, H., Zhang, T., Zhang, Y.: Stability and bifurcation analysis of delay coupled Van der Pol-Duffing oscillators. *Nonlinear Dyn.* **75**, 35–47 (2014)
43. Gattulli, V., Di Fabio, F., Luongo, A.: One to one resonant double Hopf bifurcation in aeroelastic oscillators with tuned mass dampers. *J. Sound Vib.* **262**(2), 201–217 (2003)

44. Habib, G., Kerschen, G.: Stability and bifurcation analysis of a Van der Pol-Duffing oscillator with a nonlinear tuned vibration absorber. In: Proceedings of the Eighth European Nonlinear Dynamics Conference. Vienna, Austria (2014)
45. Mansour, W.M.: Quenching of limit cycles of a van der Pol oscillator. *J. Sound Vib.* **25**(3), 395–405 (1972)
46. Suchorsky, M.K., Rand, R.H.: A pair of van der Pol oscillators coupled by fractional derivatives. *Nonlinear Dyn.* **69**, 313–324 (2012)
47. Pastor, I., Pérez-García, V.M., Encinas-Sanz, F., Guerra, J.M.: Ordered and chaotic behavior of two coupled van der Pol oscillators. *Phys. Rev. E* **48**, 171–182 (1993)
48. Teufel, A., Steindl, A., Troger, H.: Synchronization of two flow excited pendula. *Commun. Nonlinear Sci. Numer. Simul.* **11**(5), 577–594 (2006)
49. Kuznetsov, A.P., Roman, J.P.: Properties of synchronization in the systems of non-identical coupled van der Pol and van der Pol-Duffing oscillators. Broadband synchronization. *Phys. D* **238**(16), 1499–1506 (2009)
50. Paccosi, R.G., Figliola, A., Galán-Vioque, J.: A bifurcation approach to the synchronization of coupled van der Pol oscillators. *SIAM J. Appl. Dyn. Syst.* **13**(3), 1152–1167 (2014)
51. Li, X., Ji, J.C., Hansen, C.H.: Dynamics of two delay coupled van der Pol oscillators. *Mech. Res. Commun.* **33**(5), 614–627 (2006)
52. Woafu, P., Chedjou, J.C., Fotsin, H.B.: Dynamics of a system consisting of a van der Pol oscillator coupled to a Duffing oscillator. *Phys. Rev. E* **54**(6), 5929–5934 (1996)
53. Rajasekar, S., Murali, K.: Resonance behaviour and jump phenomenon in a two coupled Duffing-van der Pol oscillators. *Chaos Solitons Fractals* **19**(4), 925–934 (2004)
54. Kuznetsov, A.P., Stankevich, N.V., Turukina, L.V.: Coupled van der Pol-Duffing oscillators: Phase dynamics and structure of synchronization tongues. *Phys. D* **238**(14), 1203–1215 (2009)
55. Chatterjee, S., Dey, S.: Nonlinear dynamics of two harmonic oscillators coupled by Rayleigh type self-exciting force. *Nonlinear Dyn.* **72**, 113–128 (2013)
56. Gendelman, O.V., Bar, T.: Bifurcations of self-excitation regimes in a Van der Pol oscillator with a nonlinear energy sink. *Phys. D* **239**(3–4), 220–229 (2010)
57. Domany, E., Gendelman, O.V.: Dynamic responses and mitigation of limit cycle oscillations in Van der Pol-Duffing oscillator with nonlinear energy sink. *J. Sound Vib.* **332**(21), 5489–5507 (2013)
58. Natsiavas, S., Bouzakis, K.D., Aichouh, P.: Free vibration in a class of self-excited oscillators with 1:3 internal resonance. *Nonlinear Dyn.* **12**, 109–128 (1997)
59. Natsiavas, S., Metallidis, P.: External primary resonance of self-excited oscillators with 1:3 internal resonance. *J. Sound Vib.* **208**(2), 211–224 (1997)
60. El-Badawy, A.A., Nasr El-Deen, T.N.: Quadratic nonlinear control of a self-excited oscillator. *J. Vib. Control* **13**(4), 403–414 (2007)
61. Verros, G., Natsiavas, S.: Self-excited oscillators with asymmetric nonlinearities and one-to-two internal resonance. *Nonlinear Dyn.* **17**, 325–346 (1998)
62. Kengne, J., Chedjou, J.C., Kom, M., Kyamakya, K., Kamdoun Tamba, V.: Regular oscillations, chaos, and multi-stability in a system of two coupled van der Pol oscillators: numerical and experimental studies. *Nonlinear Dyn.* **76**, 1119–1132 (2014)
63. Chedjou, J.C., Fotsin, H.B., Woafu, P., Domngang, S.: Analog simulation of the dynamics of a van der Pol oscillator coupled to a Duffing oscillator. *IEEE Trans. Circuits Syst. I Fundam. Theory Appl.* **48**(6), 748–757 (2001)
64. Ngamsa Tegnitsap, J.V., Fotsin, H.B., Kamdoun Tamba, V., Megam Ngouonkadi, E.B.: Dynamical study of VDPCL oscillator: antimonotonicity, bursting oscillations, coexisting attractors and hardware experiments. *Eur. Phys. J. Plus* **135**, 591 (2020)

Publisher's Note Springer Nature remains neutral with regard to jurisdictional claims in published maps and institutional affiliations.

Springer Nature or its licensor (e.g. a society or other partner) holds exclusive rights to this article under a publishing agreement with the author(s) or other rightsholder(s); author self-archiving of the accepted manuscript version of this article is solely governed by the terms of such publishing agreement and applicable law.